POTENTIAL OF CONTROLLING SUBCOOLING IN RESIDENTIAL AIR CONDITIONING SYSTEM

BY

LIHAN XU

THESIS

Submitted in partial fulfillment of the requirements
for the degree of Master of Science in Mechanical Engineering
in the Graduate College of the
University of Illinois at Urbana-Champaign, 2014

Urbana, Illinois

Adviser:

Professor Predrag S. Hrnjak

ABSTRACT

This work presents an experimental and simulation study of one way of improving residential air-conditioning (RAC) system performance by controlling subcooling. Instead of conventional superheat control at evaporator outlet, condenser subcooling is monitored and controlled and the corresponding effects on vapor-compression system performance as well as the sensitivity of subcooling control to different operating conditions and different condenser sizes are discussed. Both experimental and simulation study indicate that there is COP maximizing subcooling due to trade-off of increasing cooling effect and increasing specific compression work as condenser subcooling increases.

In the experimental investigation, the potential of performance improvement (COP and cooling capacity Q) by controlling subcooling using EXV is quantified and compared to superheat controlled TXV system. The maximum of 33.0% COP improvement and 14.7% capacity gain is achieved at the same optimum subcooling, benefited from both subcooling control and improved evaporator effectiveness. It is also found that COP maximizing subcooling is a function of ambient temperature T_{cai}: COP maximizing subcooling temperature increases with increasing ambient temperature.

In the simulation investigation, the potential of performance improvement by controlling subcooling is also identified. Both COP and Q maximizing subcooling increase with increasing T_{cai}. In addition, the effect of condenser size on subcooling controlled system performance is evaluated and the results indicated that smaller size of condenser is more sensitive to change of condenser subcooling. COP or Q maximizing subcooling decreases with increasing condenser size.

Combining the simulation and experimental results, subcooling effect and condenser size effect are both interpreted as effects of condenser air refrigerant temperature difference ΔT_{in} and attempts are made to quantify the linear relationship between ΔT_{in} and COP (or Q) maximizing subcooling ΔT_{sub}. With the correlations of COP and Q maximizing subcooling, a control strategy using EXV (electronic expansion valve) with ΔT_{in} as input signal for controlling subcooling (adjusting the EXV opening) is proposed to provide COP or cooling capacity Q maximizing subcooling for the RAC system as conditions change.

To my parents

ACKNOWLEDGEMENTS

The first acknowledgement goes to the Air Conditioning and Refrigeration Center (ACRC) at the University of Illinois at Urbana-Champaign, without the support of the center, this project would not be possible. My great gratitude goes to my research adviser Prof. Predrag S. Hrnjak, who has always been supportive and helpful to me. He guided me through all the difficult times during my research.

I would like to thank my colleagues Huize Li, Hanfei Tuo, Shenghan Jin, Neal Lawrence, Yang Zou, Lili Feng and Jiu Xu for their help on facility building, model construction and valuable suggestions or comments from time to time.

I would also like to thank my best friend Min Zhang, Yuangeng Zhang and many other friends for always being by my side whenever I need them. I appreciate every moment spent with them and their encouragements are the strength that keeps me going bravely.

Finally, I would like to thank my parents for their love and support. They are always being supportive to all my decisions and their trust helps me to develop my self-recognition.

TABLE OF CONTENTS

LIST OF FIGURES

LIST OF TABLES

Nomenclature

COP	coefficient of performance	(-)	**Subscript**	
q	specific enthalpy difference across the evaporator	(kJ/kg)	e	evaporator
Q	cooling capacity	(kW)	c	condenser
w	specific compression work	(kJ/kg)	cpr	compressor
W	power	(kW)	in	air refrigerant difference
ṁ	mass flow rate	(kg/s)		
TXV	thermostatic expansion valve		sub	subcooling
EXV	electronic expansion valve		sup	superheat
fpi	fins per inch	(-)	evap	evaporating
HTC	heat transfer coefficient	(kW/m^2-k)	cond	condensing
HX	heat exchanger		a	air-side
T	temperature	(℃)	r	refrigerant-side
ΔT	temperature difference	(℃)	i	inlet
RH	relative humidity	(-)	o	outlet
AFR	air flow rate	(m^3/s)		
A	condenser area of simulation system	(m^2)		
A1	condenser area of experimental system	(m^2)		
ε	evaporator effectiveness			
x	vapor quality			
RAC	residential air-conditioning system			
MAC	mobile air-conditioning system			
SCFM	standard cubic feet per minute			
EWB	indoor entering air wet bulb temperature	(℃)		

CHAPTER 1-INTRODUCTION

1.1 Motivation

The potential for improving the system performance by controlling subcooling has already been investigated by Pottker and Hrnjak (2014) who showed that condenser subcooling can improve the mobile air-conditioning (MAC) system efficiency by 9% and 19% using R134a and R1234yf, respectively. In that study, evaporator and condenser air inlet temperature were 30℃ and 35℃ and were kept constant. The degree of subcooling was varied from 0 ℃ to 18℃ by adding refrigerant charge to the system. The results showed that there was a COP maximizing condenser subcooling for both refrigerants, at 9℃ for R134a and 11℃ for R1234yf.

The objective of this study is to expand the study by Pottker and Hrnjak (2014) to residential air-conditioning (RAC) system with both numerical and experimental investigations. The potential of controlling subcooling to improve system performance will be quantified and compared to conventional superheat controlled RAC system. Also, how does the system with subcooling control react to different operating conditions? What is the relationship between size of condenser and subcooling controlled COP improvement? What reasons are contributing to the efficiency improvement by subcooling control? All these questions will be addressed in this study. In addition, this study will present a control strategy using EXV (electronic expansion valve) for achieving COP or cooling capacity maximizing subcooling. Correlations used for the control strategy will be proposed using both simulation and experimental results.

1.2 Background

The mechanism of the way subcooling affects the vapor-compression refrigeration cycle is explained by comparing cycles with and without subcooling on a T-h diagram (Figure 1.1). The blue solid line represents the refrigeration cycle without subcooling while the red dash line represents cycle with subcooling. For cycle without subcooling, the specific enthalpy change of evaporation is denoted by q (from 5 to 2) and specific compression work is denoted by w (from 2 to 3). 1 to 2 represents the evaporator superheat region. When subcooling is present in condenser, it results in both higher condensing temperature and lower refrigerant temperature at condenser outlet. Higher condensing temperature is mainly due to the reduction of the two-phase condensation region, and it consequently increases the specific compression work by Δw. The lower condenser exit temperature results in an increment in specific enthalpy difference by Δq. The increments Δq and Δw will change as subcooling varies. Considering the system efficiency, COP of cycle without subcooling is q/w while it is $(q + \Delta q)/(w + \Delta w)$ for cycle with subcooling. Therefore, the two effects compete; subcooling effect on system performance is the trade-off between the higher cooling capacity and higher compression work.

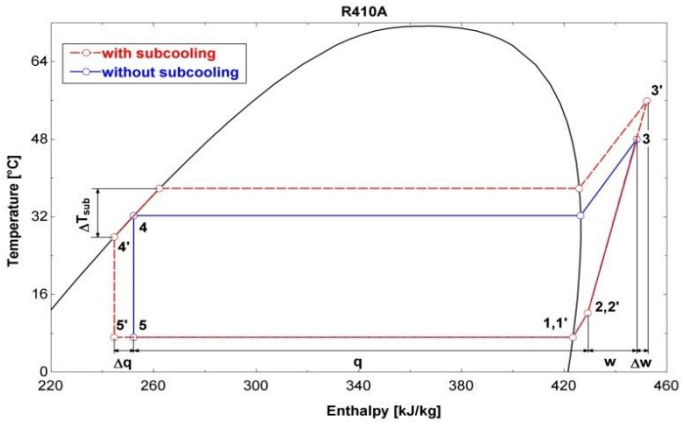

Figure 1.1: Temperature-specific enthalpy diagram of vapor-compression refrigeration cycle with/without subcooling

CHAPTER 2- EXPERIMENTAL FACILITY AND SYSTEM DESCRIPTION

2.1 Experimental facility

The testing facility used for this study consist of two insulated environmental chambers that can maintain outdoor and indoor temperature within ± 0.5°C and absolute humidity ±2%. All the connecting tubes and wind tunnels were also thermally insulated to lower the transmission heat losses.

A variable speed wind tunnel in each chamber simulates the range of operating conditions encountered in real applications. A detailed schematic of the test facility is shown in Figure 2.1.

There is also coolant (glycol) loop that goes through both outdoor and indoor chambers which can cool the chamber temperature. A PID controlled electrical heater was installed in the wind tunnel of both chambers to maintain the chamber temperature to a set point. Dehumidifiers and dew-point monitors were also utilized in the indoor chamber to ensure dry operations throughout all the testing.

Cooling capacity was obtained and balanced by both refrigerant side and air side independently. For refrigerant side, cooling capacity was calculated using refrigerant mass flow rate and refrigerant enthalpies across evaporator. Refrigerant mass flow rate was measured using a Coriolis-type mass flow meter located in the liquid line after condenser. Immersion T-type thermocouples together with pressure transducers at inlet and outlet of heat exchanger allow for refrigerant enthalpy calculation. For air-side capacity, air flow rate was calculated from nozzle differential pressure drop and air properties while air temperatures at upstream and downstream of heat exchangers as well as at nozzle exit were measured by T-type thermocouple grids. All the electrical energy inputs such as compressor power, blower powers and heater powers were

measured separately using watts transducer within ±0.2% of accuracy. Using uncertainty propagation built-in program in EES (2014), the experimental uncertainty for both air and refrigerant cooling capacity are around ±3% (±0.2 kW) and COP uncertainty is calculated to be ±5%.

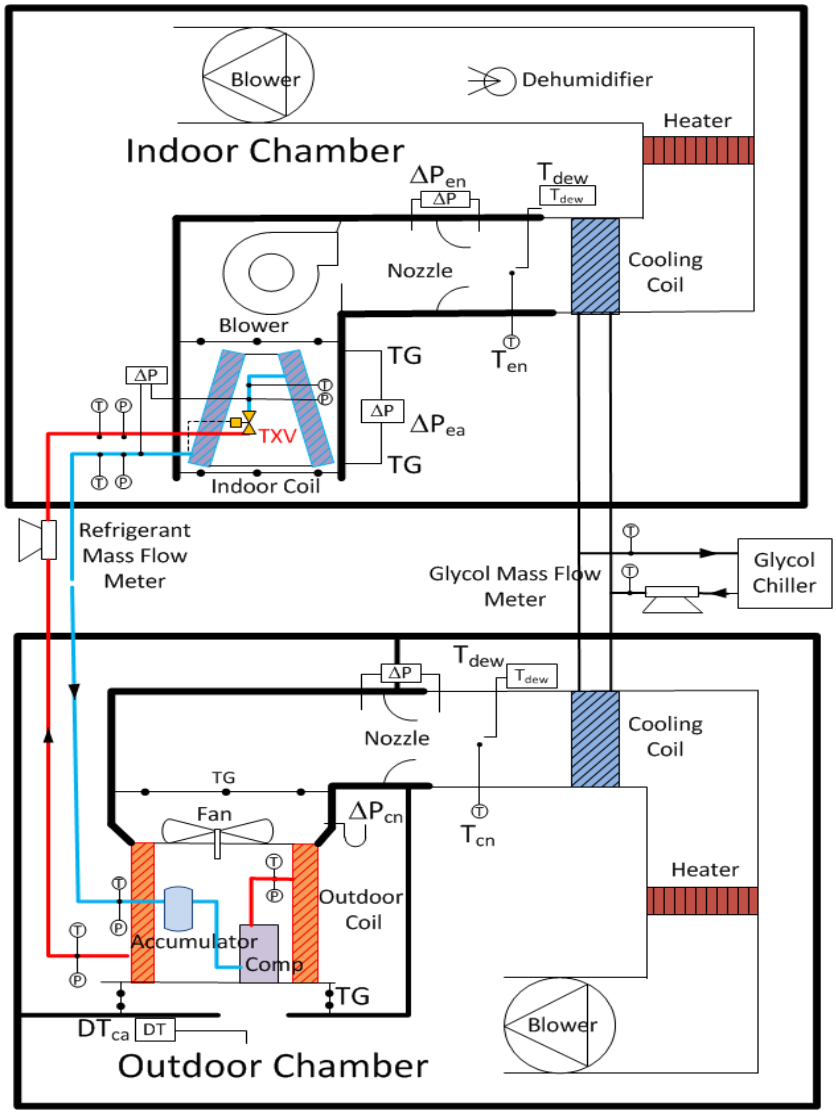

Figure 2.1: Experimental facility

2.2 AC system description

The components of the 2 Ton (7 kW) off the shelf residential A/C system (Figure 2.2) studied in this paper are a high efficiency round-tube A-coil evaporator with installed TXV (thermostatic expansion valve) and a round-tube R410A A/C & H/P outdoor coil with a variable speed hermetic scroll compressor and a low pressure side accumulator between evaporator and compressor sit inside. The compressor speed can be adjusted in percentage (i.e. from maximum of 100% to a minimum of 62%) using a factory user interface. The accumulator used is J shape type with a small hole at the bottom of the J shape tube for oil return. At steady state when liquid and vapor reaches equilibrium, the vapor quality at compressor inlet will always be a little bit less than 1 depending on the oil circulation rate.

The specifications of the evaporator and condenser are listed in Table 2.1.

Table 2.1: A/C system component specifications

	Condenser	**Evaporator**
Description	Two row, eight circuits, fin pitch 1.27 mm (20 fpi)	Two slabs, three staggered rows, eight circuits, fin pitch 1.75 mm (14.5 fpi)
Face area	2.81 m^2 (30.25 ft^2)	0.689 m^2 (7.42 ft^2)
Core depth	0.038 m	0.056 m
Core volume	0.1068 m^3	0.03858 m^3
Airside area	153.63 m^2	40.1 m^2
Ref. side area	4.61 m^2	2.39 m^2
Material	Aluminum louvered fins, copper tubes, vapor line OD=22.2 mm, liquid line OD=9.5 mm	Aluminum louvered fins, copper tubes, vapor line OD=22.2 mm, liquid line OD=9.5 mm

Figure 2.2: Pictures of indoor and outdoor heat exchangers (from left to right: indoor A-coil, outdoor coil)

The EXV (electronic expansion valve) used for replacing with TXV in subcooling tests is shown in Figure 2.3. It is a 3 ton (10.5 kW) electronically operated step motor flow control valve with total of 2500 steps. It can be operated at a speed of 1 step/time which enables for precision control of the valve opening.

Figure 2.3: EXV (electronic expansion valve)

CHAPTER 3- EXPERIMENTAL RESULTS AND DISCUSSION

3.1 System validation

The experimental system performance was first validated by comparing with provided manufacture data. The system was first charged with 7kg of refrigerant R410A by following the standard charging procedure, i.e. by matching the pre-determined subcooling for the system. And then the system was tested followed every details of the testing matrix (Table 3.1): Indoor entering air wet bulb temperature was varied to be 13.9 ℃ and 16.7℃ while for each indoor air wet bulb temperature, condenser entering air temperature was varied from 23.9℃ to 46.1℃. Outdoor air flow rate was kept to be 2300 SCFM (1.085 m^3/s) while indoor air flow rate ranges from 751 to 900 SCFM (0.353 m^3/s to 0.425 m^3/s) depending on the conditions. Compressor speed was kept to be at maximum (100%) for all the operating conditions except when capacity was held constant. The performance validation results were shown in Figure 3.1, showing good agreement of the experimental results and the manufacturer's data for all the conditions tested. COP of the system decreases as ambient air temperature increases as a result of both increasing compression work and decreasing cooling capacity.

Table 3.1: Test matrix for system validation

Evap Air	**Condenser entering air temperatures** °F **(**℃**)**				
	75 (23.9)	85 (29.4)	95 (35)	105 (40.6)	115 (46.1)
EWB °F **(**℃**)**	**AFR (indoor) [SCFM]**	**AFR (indoor) [SCFM]**	**AFR (indoor) [SCFM]**	**AFR (indoor) [SCFM]**	**AFR (indoor) [SCFM]**
57 (13.9)	887	875	900	751	825
62 (16.7)	887	875	900	751	825

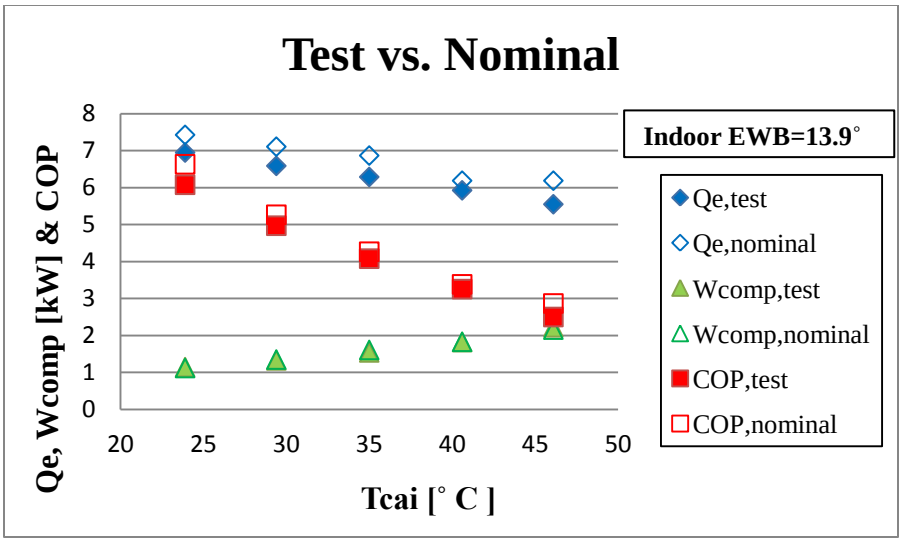

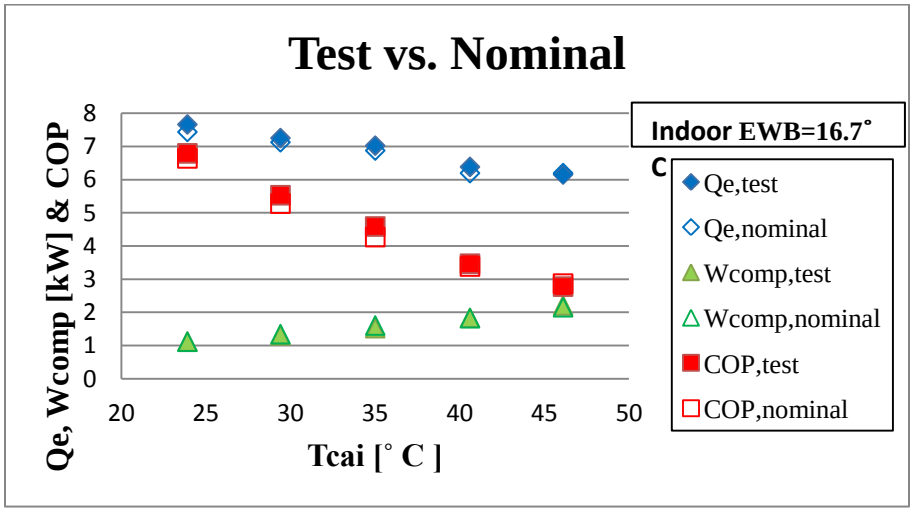

Figure 3.1: Performance comparison between test and manufacture data
(a) Indoor EWB= 13.9℃ (b) Indoor EWB=16.7℃

3.2 Baseline with TXV

Baseline tests were conducted using the installed TXV to determine the performance and subcooling under normal operations. Table 3.2 summarizes the test matrix. Indoor temperature T_{eai} was kept to be 20 ˚C, ambient temperature T_{cai} was varied from 20 ˚C to 40 ˚C. Indoor air flow rate was kept to be 900 SCFM (0.425 m^3/s) while outdoor air flow rate was maintained at 2300 SCFM (1.085 m^3/s). Superheat at evaporator outlet was controlled to be 3 ˚C by TXV.

Figure 3.2 shows the baseline results. The blue line represents the assumed load requirement by the house. It is assumed to be a linear line. At ambient temperature of 20 ˚C, load is 0 and the system does not require cooling while at ambient temperature of 40 ˚C which is the highest design condition for central areas according to ASHARE standard, the house should be at its maximum load. The red line is the actual system capacity curve performed by the system at reduced compressor speed. Also, subcooling at T_{cai} equals to 35 ˚C, 38 ˚C and 40 ˚C was obtained to see how much potential the system have for subcooling control. More details of the baseline performance including capacities, compressor work, refrigerant mass flow rate, superheat at evaporator outlet, subcooling at condenser outlet and COP were shown in Figure 3.3. COP decreases with increasing ambient temperatures due to faster increase in compression work than evaporator capacity.

Table 3.2: Test matrix for baseline with TXV

Test	**T_{eai} (˚C)**	**T_{cai} (˚C)**	**AFR (indoor) [SCFM/ m^3/s]**	**AFR (outdoor) [SCFM/ m^3/s]**	**Compressor speed %**	**ΔT_{sup} [℃]**
D	20	35	900/0.425	2300/1.085	65	3.0
E	20	38	900/0.425	2300/1.085	85	3.0
F	20	40	900/0.425	2300/1.085	100	3.0

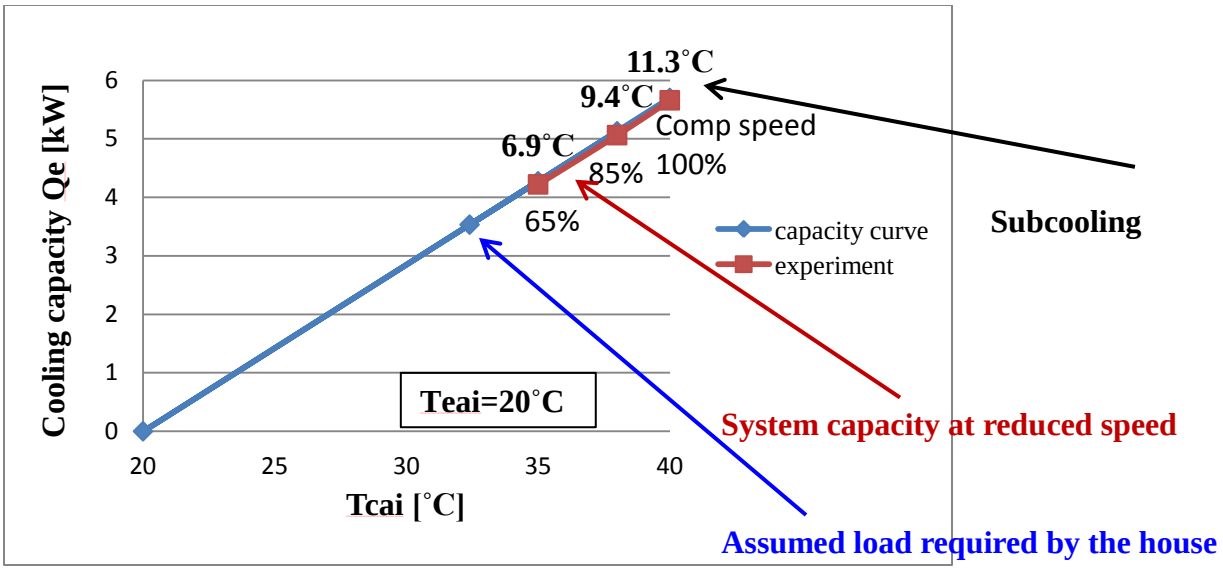

Figure 3.2: Determination of performance and subcooling with TXV system

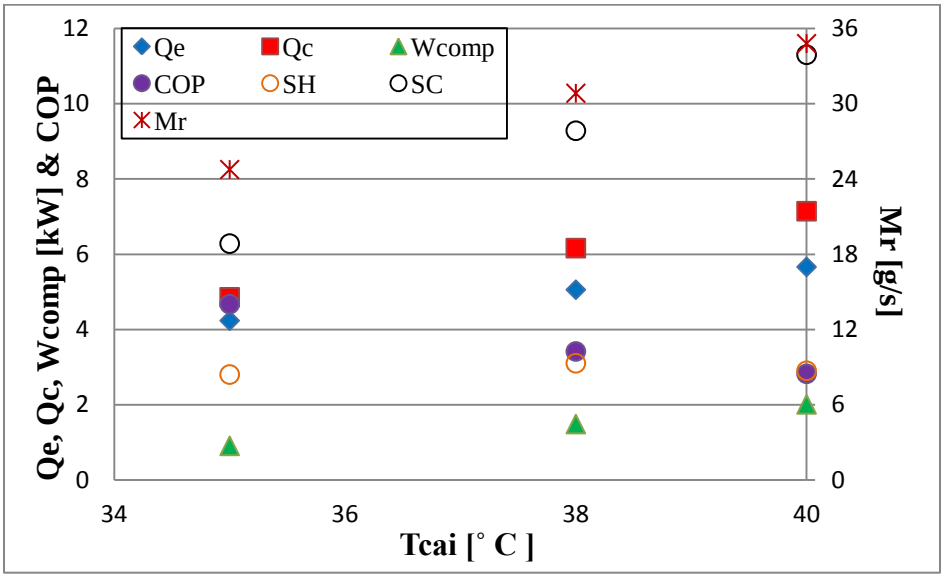

Figure 3.3: Detailed baseline performance with TXV system

3.3 Subcooling test with EXV

The system configuration was modified to replace TXV (thermostatic expansion valve) between condenser and evaporator with EXV (electronic expansion valve) for the subcooling control tests. In this study, condenser subcooling is the active control instead of superheat control at

evaporator outlet. Condenser subcooling was obtained by adjusting the opening of EXV (electronic expansion valve). When the valve opening was adjusted in the way of closing it more, subcooling in condenser will increase due to increasing condensing pressure and thus reduce the two phase region in the heat exchanger to accommodate the increase of subcooled liquid refrigerant at condenser exit. On the contrary, condenser subcooling will decrease as the valve opening was adjusted in the way of opening it more. Since superheat was not controlled in experiments, a low pressure side receiver (accumulator) was added between evaporator and compressor to ensure the reliability of compressor.

For each operating conditions in Table 3.2, air inlet temperatures, volumetric flow rates and compressor speed were kept constant as TXV tests. The opening of EXV was adjusted to obtain different condenser subcooling. As valve opening increases, condensing pressure decreases and as a result the compressor compression work reduces; in the meanwhile, the smaller condenser subcooling results in higher refrigerant enthalpy at condenser outlet which increases the evaporator inlet vapor quality and thus reducing the refrigerating effect (specific enthalpy difference across the evaporator). On the other hand, refrigerant mass flow rate increases with the valve opening. Therefore, cooling capacity changes as the result of the trade-off between decreasing evaporator specific enthalpy difference and increasing refrigerant mass flow rate. The change of cooling capacity is shown in Figure 3.4, represented by hollow triangles. Capacity reaches maximum at subcooling of 4.94 ˚C, 4.35 ˚C and 3.10 ˚C for T_{cai} equals to 40 ˚C, 38 ˚C and 35 ˚C, respectively. Comparing with TXV baseline, cooling capacity was raised by 14.7%, 10.5% and 9.9%, respectively. Figure 3.4 also shows the trend of COP (represented by solid diamonds) as condenser subcooling increases, which is the integrated result of cooling capacity and compression work. For each operating condition, there is COP maximizing subcooling and

the COP improvement by controlling subcooling using EXV compared to TXV baseline is 33.0%, 24.0% and 18.6% for T_{cai} equals to 40 ˚C, 38 ˚C and 35 ˚C, respectively. COP reaches its maximum at the same optimum subcooling for maximizing cooling capacity. In other words, the system is at its best performance, maximum COP and maximum cooling capacity simultaneously, at subcooling of 4.94 ˚C, 4.35 ˚C and 3.10 ˚C for T_{cai} equals to 40 ˚C, 38 ˚C and 35 ˚C. The detailed comparison of the subcooling controlled (EXV) system performance with baseline (TXV) is listed in Table 3.3.

In addition to constant compressor speed case, another set of subcooling tests were conducted with cooling capacity constant as TXV baseline by adjusting the compressor speed. Due to the restriction of compressor speed range (62% to 100%) which is preset by manufacturer, the tests can only achieve limited range of subcooling and COP maximizing subcooling was not observed. As indicated in Figure 3.5, COP increases with decreasing subcooling and there is plenty of room for COP improvement by controlling subcooling compared with TXV baseline.

Table 3.3: Performance comparison between COP maximizing EXV and TXV system

$\mathbf{T_{cai}}$ (˚C)	40		38		35	
	EXV	**TXV**	**EXV**	**TXV**	**EXV**	**TXV**
$\mathbf{Q_e}$ [kW]	6.49	5.66	5.58	5.05	4.65	4.23
$\mathbf{W_{cpr}}$ [kW]	1.73	2.007	1.318	1.484	0.8379	0.904
$\mathbf{T_{evap}}$ [˚C]	8.012	6.111	8.63	7.145	10.81	9.778
$\mathbf{T_{cond}}$ [˚C]	47.57	52.77	44.76	48.59	40.31	42.23
$\Delta\mathbf{T_{sup}}$ [˚C]	0.5	2.9	0.9	3.1	0.8	2.8
$\Delta\mathbf{T_{sub}}$ [˚C]	4.94	11.3	4.35	9.28	3.10	6.28
COP	3.75	2.82	4.23	3.41	5.55	4.68

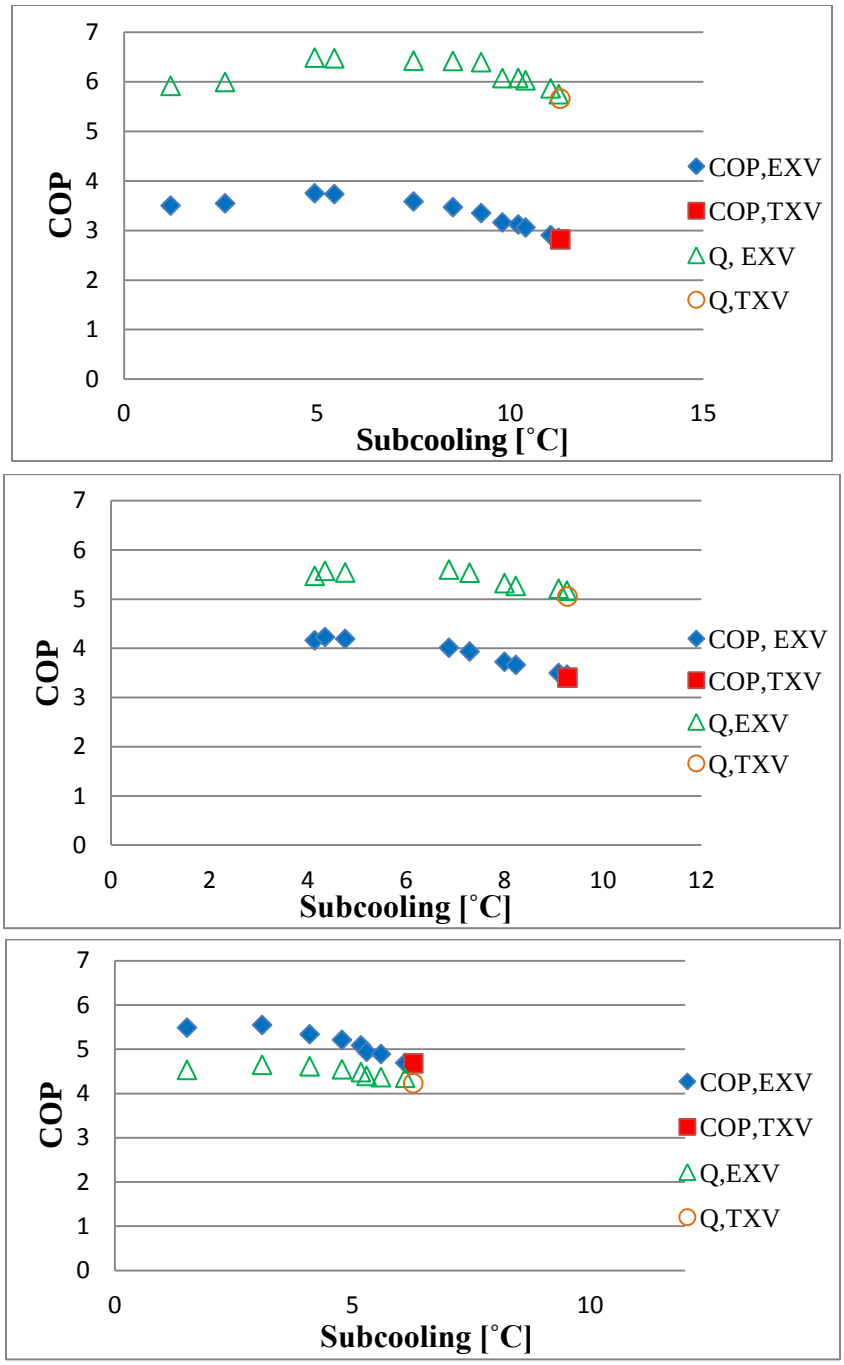

Figure 3.4: Performance **(**COP and Q) improved compared to TXV control by adjusting subcooling (at constant compressor speed)

(a) T_{cai}=40 ˚C, T_{eai}=20 ˚C (b) T_{cai}=38 ˚C, T_{eai}=20 ˚C (c) T_{cai}=35 ˚C, T_{eai}=20 ˚C

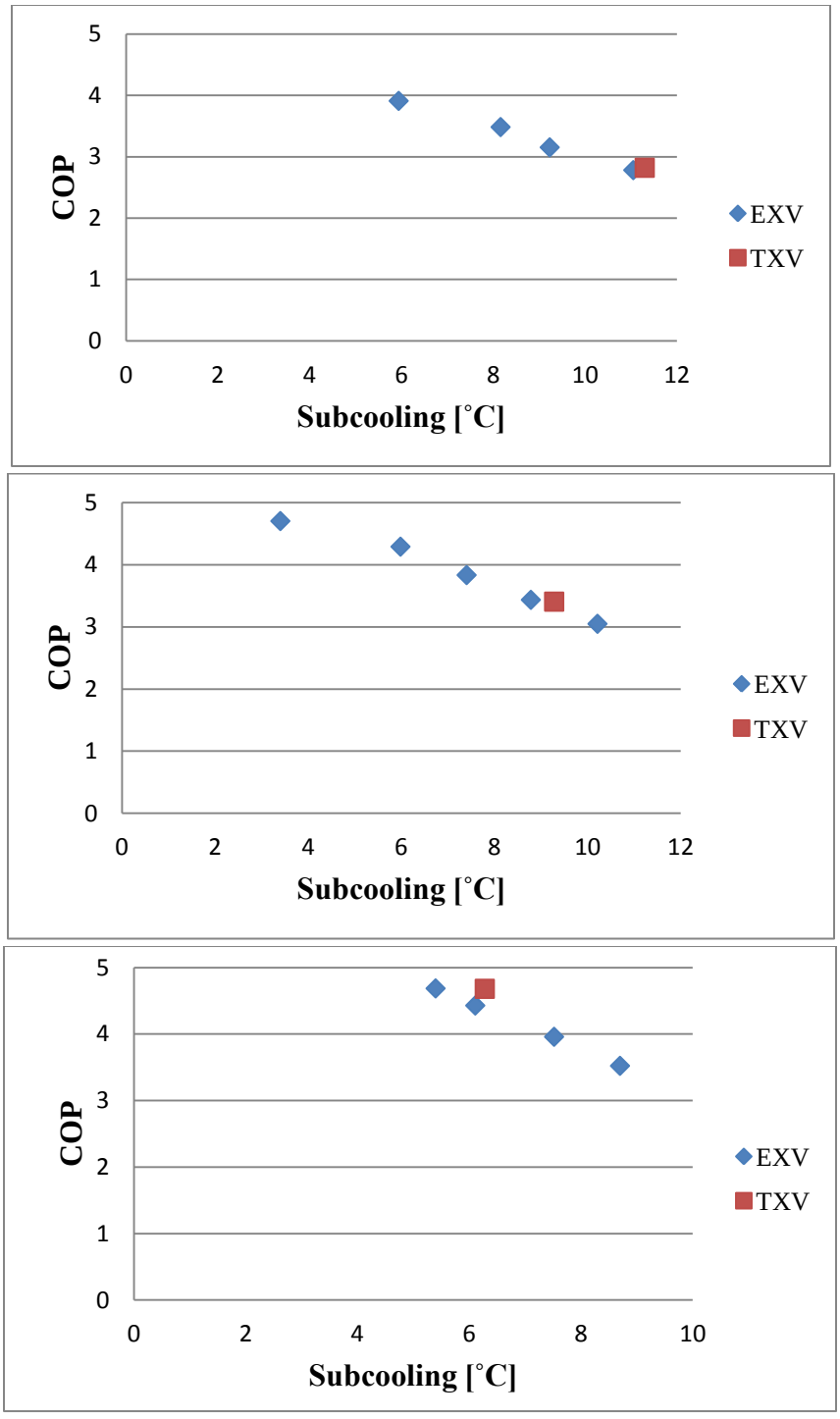

Figure 3.5: Efficiency (COP) further improved when cooling capacity is held constant

(a) T_{cai}=40 ˚C, T_{eai}=20 ˚C (b) T_{cai}=38 ˚C, T_{eai}=20 ˚C (c) T_{cai}=35 ˚C, T_{eai}=20 ˚C

3.4 Discussion

Results presented above show maximum of 33.0% increase in COP and 14.7% gain in cooling capacity Q at the same optimum subcooling when controlling subcooling using EXV compared with TXV baseline. The huge improvement is achieved both by controlling subcooling (cycle) and by improving evaporator effectiveness due to reduction of dry-out/superheated zone.

Figure 3.6 presents evaporator effectiveness as a function of evaporator outlet superheat. As shown, from 3˚C of superheat (where TXV controlled system is at) to 0.5 ˚C (where evaporator outlet is probably in two-phase considering ± 0.5°C temperature measurement uncertainty), the effectiveness of the heat exchanger has been improved from 0.6 to 0.9. Figure 3.7 presents the change of evaporator outlet superheat and vapor quality with condenser subcooling. When condenser subcooling is at 11.3°C (that is the value TXV controlled system set), superheat is 3 ˚C and evaporator outlet is in the superheat zone. In this zone, evaporator effectiveness is less than ideal as indicated in Figure 3.6. As condenser subcooling decreases, superheat decreases with it and it reaches the slightly wet zone which is highlighted by a circle in Figure 3.7, where evaporator outlet quality is slightly below 1. This region is ideal for system operation because it is good for both evaporator and compressor, evaporator effectiveness is better since no superheat or dry-out is present; compressor reliability is ensured because no liquid refrigerant goes into compressor. Also, the optimal condenser subcooling (4.94 °C for the operating condition discussed) is happened to be in this zone. If condenser subcooling continues to decrease, the evaporator outlet is at two-phase region and cooling effect of liquid refrigerant that goes to compressor is lost.

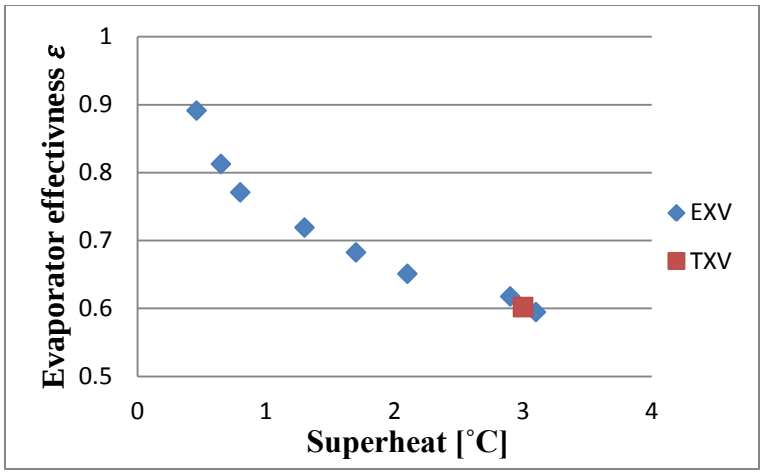

Figure 3.6: Evaporator effectiveness ε is improved as superheat reduces (condition: T_{cai}=40 ˚C, T_{eai}=20 ˚C)

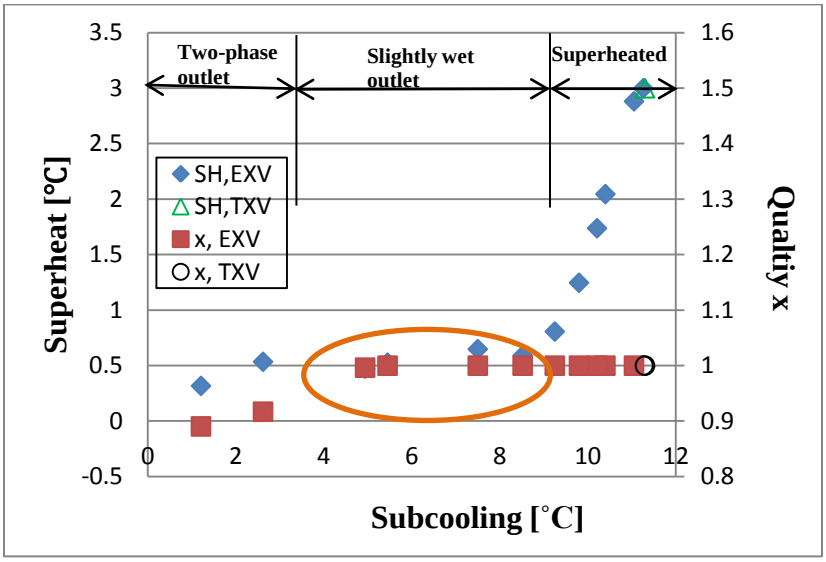

Figure 3.7: Situation in the evaporator as subcooling controller searches for the highest efficiency
(T_{cai}=40 ˚C, T_{eai}=20 ˚C)

Figure 3.8 shows the comparison of EXV and TXV controlled system at T_{cai}=40 ˚C, T_{eai}=20 ˚C. As shown in the figure, the COP maximizing subcooling is 4.94 ˚C, much smaller than 11.3 ˚C found in superheat controlled TXV system. The EXV controlled system can achieve smaller (COP maximizing) subcooling that results in lowering condensation pressure and providing

larger two-phase heat transfer area in condenser. Lower condensing pressure also results in reduction of compression work. As mentioned, the evaporator exit before the low-pressure side receiver (accumulator) for subcooling controlled EXV system is in the slightly wet zone (Figure 3.7). The reduced refrigerant liquid quantity in the condenser migrates to the accumulator, which results in better distributed evaporator surface and thus higher effective evaporator.

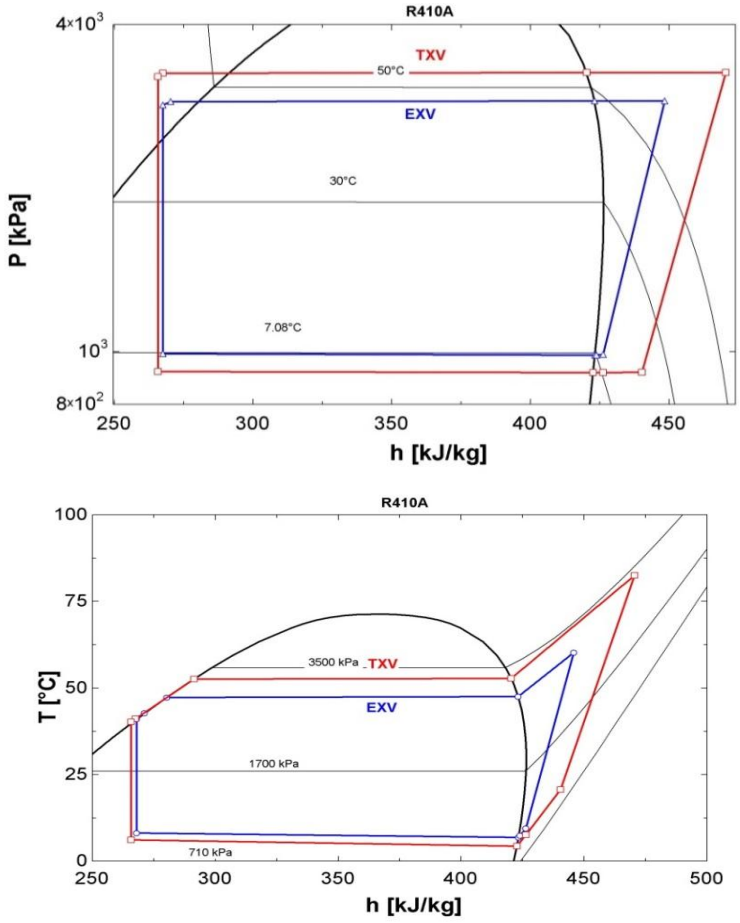

Figure 3.8: T_{cai}=40 ˚C, T_{eai}=20 ˚C

Similar results were obtained for the other two operating conditions (shown in Figure 3.9 and 3.10). But the COP maximizing condenser subcooling varied for different T_{cai}. When other conditions such as T_{eai}, air volumetric flow rates and compressor speed were kept constant, COP maximizing condenser subcooling increases with increasing ambient temperature. In normal operations of residential a/c system, charge is usually fixed to a certain amount, thus condenser subcooling may not always at COP maximizing value as the operating condition changes. In other words, if we can obtain a relationship between COP maximizing subcooling and ambient temperature, we can achieve COP maximizing subcooling using EXV or other possible methods.

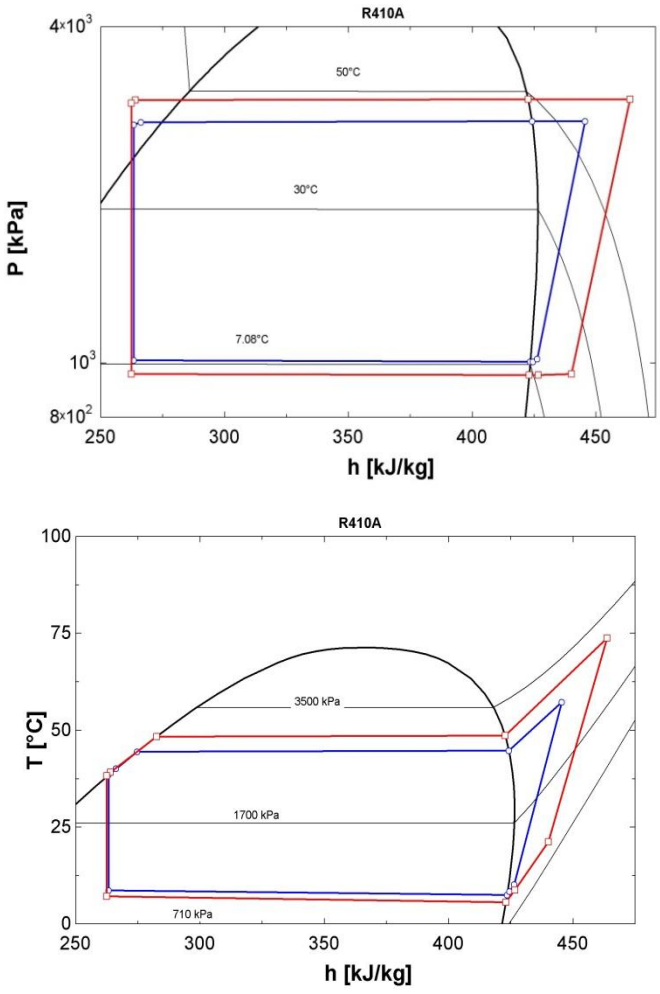

Figure 3.9: T_{cai}=38 ˚C, T_{eai}=20 ˚C

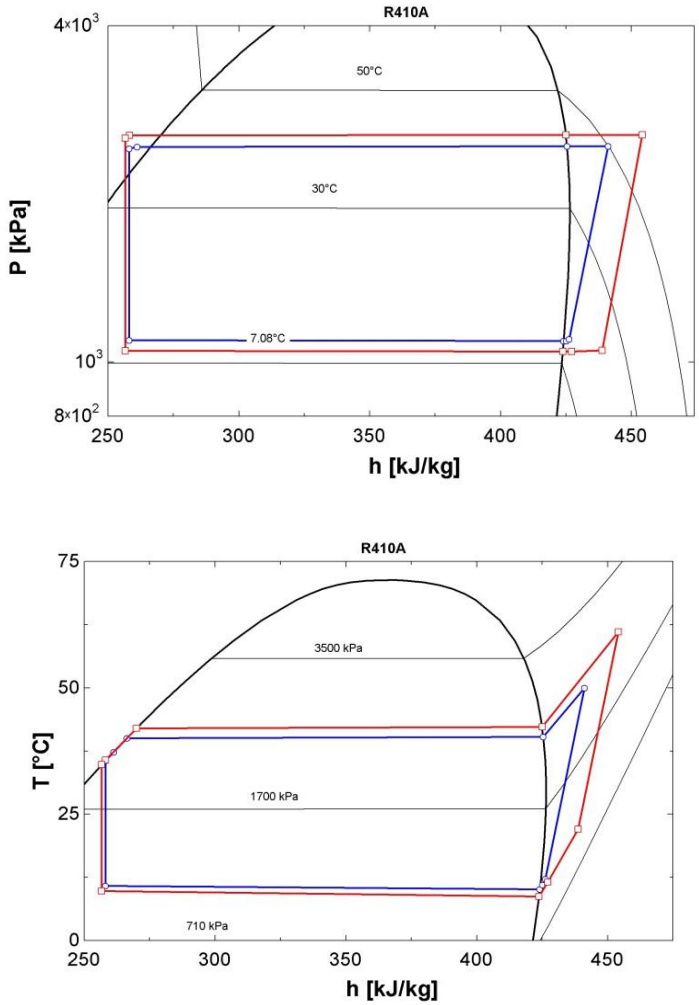

Figure 3.10: T_{cai}=35 ˚C, T_{eai}=20 ˚C

CHAPTER 4- SIMULATION MODEL

4.1 System for model development

The system used for the simulation study is a 3 Ton (10.5 kW) A/C system with a high efficiency round-tube R410A outdoor coil, a round-tube evaporator with installed TXV (thermostatic expansion valve), and a hermetic scroll compressor. The specifications of the evaporator and condenser are listed in Table 4.1 (Beaver et al., 1999).

Table 4.1: A/C system component specifications

	Condenser	**Evaporator**
Description	One row, two circuits, fin pitch 1 mm (24 fpi)	Three rows, six circuits, fin pitch 1.7 mm (14 fpi)
Face area	1.42 m^2	0.32 m^2
Core depth	0.0185 m	0.056 m
Core volume	0.026 m^3	0.018 m^3
Airside area	44.56 m^2	18.88 m^2
Ref. side area	1.58 m^2	1.08 m^2
Material	Aluminum wavy plate fins, copper tubes, OD=9.5 mm	Aluminum wavy plate fins, copper tubes, OD=9.5 mm

4.2 Model development

In order to predict the performance of the residential A/C system, a system model has been built using EES (Engineering Equation Solver, 2014). The system model contains modules simulating the four main components: condenser, expansion valve, evaporator, and compressor. They are coupled by correlating equations of pressure, enthalpy, and mass flow rate. For the heat exchangers, the finite volume method was used for calculating the heat transfer rate and pressure

drop. Each tube pass of condenser was divided into 5 elements while 3 elements per tube pass were used for the evaporator. For each element, the effectiveness-NTU method for a cross-flow heat exchanger was applied for heat transfer calculations. Detailed heat transfer and pressure drop correlations are listed in Table 4.2.

For the compressor model, the 10-parameter polynomial curve fitting method was adopted. Using the manufacturing data, mass flow rate and compressor power can be calculated. A scaling factor β was used to adjust the speed of the variable-speed compressor in the model.

The inputs to the system model are: heat exchanger and compressor geometries, air volumetric flow rate through outdoor and indoor chamber ducts, air-side inlet conditions, and degrees of superheat and subcooling. The modules run separately in a sequential order, which output thermodynamic properties such as temperature, pressure, and specific enthalpy when the system inputs were implemented.

Several other assumptions were made for the model:

1. Uniform temperature and velocity profile at air-side inlet.
2. Isenthalpic expansion process.
3. Volumetric and isentropic efficiencies are independent of compressor speed.
4. Refrigerant pressure drop in compressor discharge line and liquid line are ignored.
5. Lubricant effect is neglected (It can be improved by adopting the method introduced in Li and Hrnjak, 2013, 2014)

Table 4.2: Heat transfer and pressure drop correlations

Items	Correlations
Refrigerant-side	
Single phase HTC	Gnielinski (1976)
Condensation HTC	Cavallini et al. (2006)
Evaporation HTC	Wattelet and Chato (1994)
Single-phase pressure drop	Friction factor from Churchill (1977)
Two-phase pressure drop	Friedel (1979)
Air-side	
HTC for wavy plate fin-and-tube HX	Webb (1990)
Pressure drop for wavy plate fin-and-tube HX	Kim, Yun and Webb (1997)

4.3 Model validation

The model was then validated using experimental data from a previous study (Beaver et al., 1999). Three operating conditions were tested (listed in Table 4.3). Indoor temperature was kept to be 26.7 ℃ for all three conditions while outdoor temperature varied. Condition **A** and **B** are prescribed by ASHARE Standard 116/1995 (1995).

Table 4.3: Test conditions for simulation study

	T_{eai} [℃]	T_{cai} [℃]	RH	AFR (indoor) $[m^3/s]$	AFR (outdoor) $[m^3/s]$	ΔT_{sub} [℃]	ΔT_{sup} [℃]
A	26.7	35.0	0.506	0.57	1.33	6.9	2.9
B	26.7	27.8	0.320	0.57	1.33	6.7	3.0
C	26.7	39.0	0.504	0.57	1.33	6.3	0.6

The results from simulation and experimental data from Beaver et al. (1999) were compared in Table 4.4 for the operating conditions listed in Table 4.3. Most of the simulation results were within 2% of error while the error of saturation temperatures are within ± 1.6 ℃ .

Figure 4.1 shows model validation by comparing experimental data (blue solid line) and simulation results (red dash line) in a P-h diagram for condition **B**. Both evaporator and condenser side shows good agreement between simulation and experimental data.

Table 4.4: Model validation

	Condition A			**Condition B**			**Condition C**		
	Model	Data	Error	Model	Data	Error	Model	Data	Error
Q_e [W]	10.40	10.46	-0.57%	10.49	10.50	-0.10%	10.06	10.00	0.60%
Q_c [W]	12.93	13.10	-1.30%	12.58	12.61	-0.24%	12.85	13.01	-1.23%
W_{cpr} [W]	2.63	2.64	-0.38%	2.22	2.20	0.91%	2.86	2.88	-0.69%
T_{evap} [℃]	8.9	10.5	-1.6 ℃	6.4	7.5	-1.1 ℃	9.8	11.3	-1.5 ℃
T_{cond} [℃]	46.0	44.9	1.1 ℃	38.4	37.0	1.4 ℃	49.6	48.6	1.0 ℃
COP	3.96	3.97	-0.25%	4.72	4.76	-0.84%	3.52	3.47	1.44%

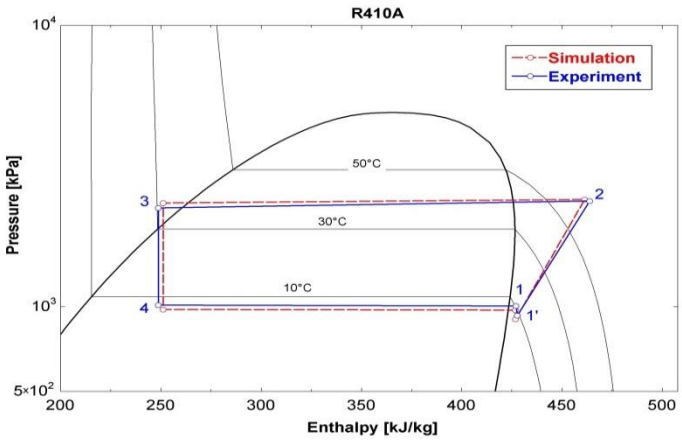

Figure 4.1: Pressure-specific enthalpy diagram (condition **B** in Table 3)

4.4 Simulation results

4.4.1 Subcooling effect

The model validated in previous section will help to analyze subcooling effects in more realistic situations than a pure thermodynamic cycle. Figure 4.2 (a) shows the effects of subcooling on normalized COP, cooling capacity, and compression work for condition **A** (Table 4.3) of the RAC system described in section 4.3. The normalization was done based on values at zero subcooling. For this operating condition, subcooling temperature was varied from 0 to 12 ℃ while air flow rate, evaporator outlet superheat, and compressor speed were kept constant. As subcooling increases from 0 to 12 ℃, both cooling capacity and compression work increase while COP experiences its maximum value at ΔT_{sub} = 6.5 ℃. The interaction between capacity and work determines the shape of the COP curve. This result confirms the cycle analysis in Chapter 1, where it was explained that increase in subcooling results in both higher condensing temperature and lower refrigerant temperature at condenser outlet, resulting in higher specific enthalpy difference in evaporator and higher specific compressor work. As subcooling increases, refrigerant mass flow rate also decreases as a consequence of lowering evaporation pressure (see Figure 4.3) and this was accounted for the cooling capacity and work calculations. The increase of cooling capacity slows down while the increase of compression work accelerates when passing the COP maximizing subcooling temperature. This indicates that subcooling has a stronger effect on cooling capacity from zero to COP maximizing subcooling and inversely for subcooling above COP maximizing value.

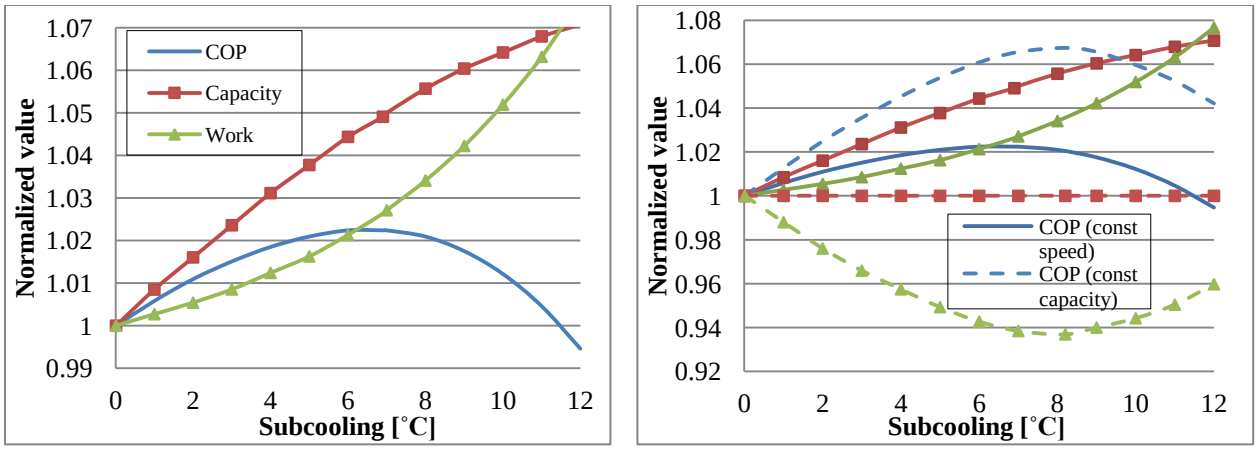

(a) (b)

Figure 4.2: (a) Effect of subcooling temperature on normalized COP, cooling capacity, and compression work for constant compressor speed; (b) Comparison of subcooling effects on normalized COP, cooling capacity and compression work for constant compressor speed and constant cooling capacity (condition **A** in Table 4.3)

A similar analysis was conducted for keeping cooling capacity constant instead of compressor speed. Capacity was matched at zero subcooling. Figure 4.2 (b) shows the comparison of subcooling effects on normalized COP, cooling capacity, and compression work of constant speed case and constant cooling capacity case. The improvement of system COP is much higher for the constant cooling capacity case than that of constant compressor speed. This is because for the constant cooling capacity case, the increase in cooling capacity when compressor speed is constant as shown in Figure 4.2 (a) is now accounted in COP improvement.

The model was also used to analyze how RAC system with subcooling control reacts to different operating conditions. Figure 4.4 presents the effect of subcooling on normalized COP for three condenser air inlet temperatures 27.8 ℃, 35℃, and 39 ℃ while evaporator air inlet temperature was kept to be 26.7 ℃ (condition **A, B, C** in Table 4.3). Subcooling temperature was varied from 0 to 12℃ while air flow rates and superheat were kept constant (specified in Table 4.3). Cooling capacity was matched at zero subcooling case for each operating condition by adjusting the

compressor speed. The three operating conditions all show the same subcooling effects on COP, but the improvements are different. The COP improvement is 7.9% (at ΔT_{sub}=9.0℃), 6.7% (at ΔT_{sub}=8.2 ℃) and 5.3% (at ΔT_{sub}=8.0℃) for T_{cai} equal to 39 ℃ , 35℃, 27.8 ℃ , respectively. Higher condenser air inlet temperature results in greater COP improvements by changing subcooling. Also, the figure indicates that COP maximizing subcooling increases with increasing T_{cai} (8.0℃, 8.2℃ and 9.0℃ for T_{cai}=27.8℃, 35℃ and 39℃ respectively).

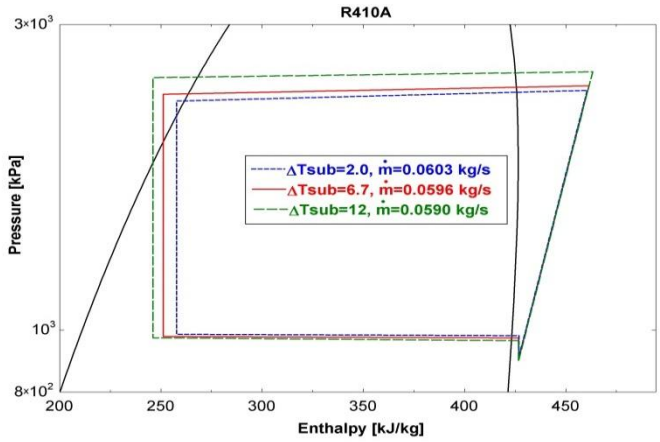

Figure 4.3: Effect of subcooling on refrigerant mass flow rates for ΔT_{sub}=2.0 ℃, 6.7 ℃, and 12 ℃

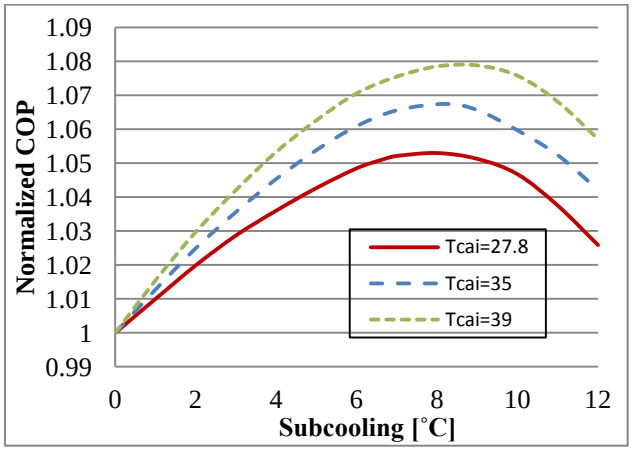

Figure 4.4: Effect of subcooling temperature on normalized COP (condition **A, B, C** in Table 4.3) for constant capacity

The simulation results indicate that the subcooling effect on RAC system performance is not as high as in MAC as predicted by Pottker and Hrnjak (2014). The main reason for that is due to the much larger condenser size in RAC compared to MAC. In fact, condenser size has a strong impact on the subcooling effect. The simulation model was used to evaluate the magnitude of the condenser size effects in the next section. It was shown in the experimental investigation of the previous chapter that real effects when controlling subcooling was actually much larger than expected due to improvements in evaporator performance as a consequence of reduced superheat/dry-out.

4.4.2 Condenser size effect

Condenser size effects on subcooling improved system efficiency was studied by varying the condenser size to be 1, 2, and 4 times the original condenser size (A) specified in system description of section 2 (air-side area A_a=44.56 m^2, refrigerant-side area A_r=1.58 m^2) by adjusting the condenser side geometry. Condenser air-side face velocity was kept constant by increasing the outdoor air volumetric flow rate by the same factor as geometry to maintain constant air-side heat transfer. The volumetric flow rate is 1.33 m^3/s. Multiplying volumetric flow rates 2 and 4 times may not be realistic in reality, but it was selected for the purpose of analyzing size effects (in addition, constant volumetric flow rate case was also conducted and the results were shown in Appendix). Everything else such as evaporator size and indoor air volumetric flow rate were kept constant. Operating condition **A, B, C** (Table 4.3) were applied for this analysis. Simulation results for condition **B** (Figure 4.5) show that larger the condenser size, smaller subcooling effect on system performance is observed. For the original condenser size, subcooling can improve the system efficiency by 5.3%, whereas for 4 times original condenser size, subcooling effect becomes detrimental to COP. Also, for different condenser

sizes, COP maximizing subcooling temperature varies. It decreases from 8.0 ℃ (original size A) to 4.0 ℃ (2 times A), then further to 0.2 ℃ (4 times A). The similar findings also apply for operating conditions **A** and **C** (shown in Appendix).

Effect of condenser size on subcooling improved cooling capacity Q was also studied. Simulation results for condition **B** (Table 4.3) are shown in Figure 4.6 (similar findings for conditions **A, C** in Appendix). Similar to COP, smaller condenser size has higher potential for increasing cooling capacity. For the original condenser size, the improvement was 5.6%, while it decreased to 2.2% as condenser size doubled, and no improvement when condenser size quadrupled. Q maximizing subcooling temperature also decreases as condenser size increases.

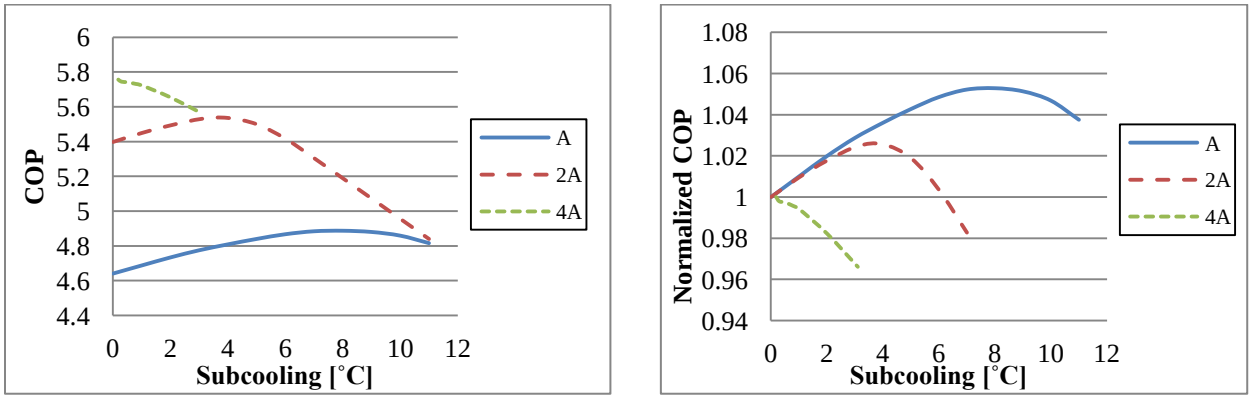

(a) (b)

Figure 4.5: Effect of condenser size on subcooling improved COP presented in (a) actual and (b) normalized terms (condition **B** in Table 4.3)

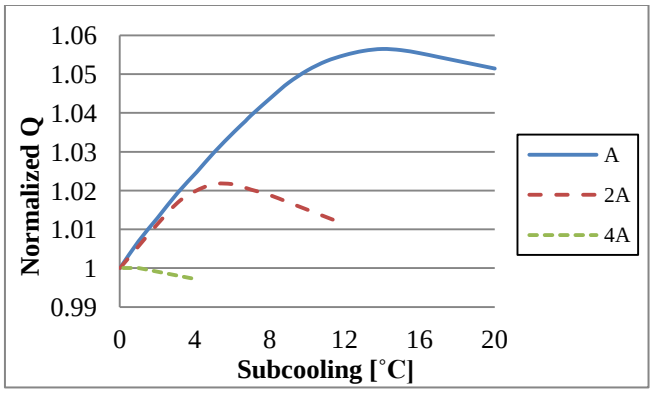

Figure 4.6: Effect of condenser size on subcooling improved cooling capacity Q presented in normalized way (condition **B** in Table 4.3)

4.5 Discussion

The numerical and experimental results both indicated that subcooling effect is a function of ambient temperature. COP maximizing subcooling increases with increasing T_{cai}. At higher ambient temperature, the heat rejection rate is greater thus allowing for greater condenser air refrigerant temperature difference ΔT_{in}, the temperature difference between ambient air and saturated refrigerant in the condenser. Higher ambient temperature results in higher ΔT_{in} and makes more room for condenser subcooling to act and consequently provides greater potential for COP or Q improvements. In fact, subcooling effects can be interpreted as effects of ΔT_{in} on subcooling improved system performance.

The numerical sensitivity tests also indicated that subcooling effect is a function of condenser sizes this is because condenser size is inversely proportional to condenser air refrigerant temperature difference ΔT_{in} assuming heat rejection rate was not changed. Smaller condenser size results in higher ΔT_{in} and greater room for performance improvement by controlling

subcooling. Follow the same analogy, condenser size effects on subcooling controlled system performance can be also interpreted as effects of ΔT_{in}.

In the next chapter, COP and Q maximizing subcooling temperature ΔT_{sub} and its corresponding condenser air refrigerant temperature difference ΔT_{in} from both simulation and experimental results will be summarized to find the relationship between them so that COP maximizing subcooling temperature ΔT_{sub} can be tracked and controlled.

CHAPTER 5- SUBCOOLING CONTROL STRATEGY

It would be reasonable to evaluate possibility in improving performance of the system (COP or capacity) by controlling subcooling. That could be achieved by controlling opening of EXV (subcooling) based on temperature difference ΔT_{in} and utilizing low-pressure receiver (accumulator) option. In this section a strategy for controlling subcooling will be discussed.

Both COP and Q maximizing subcooling temperature exhibit an inverse relationship with condenser size, i.e. direct relationship with ΔT_{in}. In fact, COP or Q maximizing subcooling can be presented as a linear function of ΔT_{in}: $\Delta \boldsymbol{T_{sub}} = \boldsymbol{A} * \Delta \boldsymbol{T_{in}} + \boldsymbol{B}$. The coefficients A and B can be determined based on available data for a certain range of conditions.

Tables 5.1 and 5.2 summarize COP and Q maximizing subcooling temperature ΔT_{sub} and its corresponding condenser air refrigerant temperature difference ΔT_{in} from simulation results for three ambient conditions **A, B, C** and three condenser sizes (1, 2 and 4 times of original area A). Table 5.3 summarizes COP maximizing subcooling temperature ΔT_{sub} and its corresponding condenser air refrigerant temperature difference ΔT_{in} from experimental results for three different ambient temperatures **D, E** and **F**.

Table 5.1: COP maximizing subcooling temperature and condenser air refrigerant temperature difference for varying condenser sizes and varying ambient conditions from simulation

Condenser size	**Condition A**		**Condition B**		**Condition C**	
	ΔT_{sub} [°C]	ΔT_{in} [°C]	ΔT_{sub} [°C]	ΔT_{in} [°C]	ΔT_{sub} [°C]	ΔT_{in} [°C]
A	8.2	11.2	8.0	10.7	9.0	11.6
2A	4.0	4.7	4.0	4.4	4.0	4.7
4A	0.3	0.2	0.2	0.3	0.4	0.5

Table 5.2: Q maximizing subcooling temperature and condenser air refrigerant temperature difference for varying condenser sizes and varying ambient conditions from simulation

Condenser size	**Condition A**		**Condition B**		**Condition C**	
	ΔT_{sub} [℃]	ΔT_{in} [℃]	ΔT_{sub} [℃]	ΔT_{in} [℃]	ΔT_{sub} [℃]	ΔT_{in} [℃]
A	16.0	16.6	14.0	14.6	18.0	18.2
2A	6.9	7.0	5.5	5.6	6.3	6.4
4A	0.9	1.0	0.2	0.3	0.6	0.8

Table 5.3: COP maximizing subcooling temperature and condenser air refrigerant temperature difference for varying ambient conditions from experiments

Condenser size	**Condition D**		**Condition E**		**Condition F**	
	ΔT_{sub} [℃]	ΔT_{in} [℃]	ΔT_{sub} [℃]	ΔT_{in} [℃]	ΔT_{sub} [℃]	ΔT_{in} [℃]
A1	2.7	5.31	4.35	6.76	4.94	7.57

5.1 Maximization of COP

Results indicate that COP maximizing subcooling can be presented as a linear function of condenser air refrigerant temperature difference ΔT_{in}: $\Delta \boldsymbol{T_{sub}} = \boldsymbol{A^*} \Delta \boldsymbol{T_{in}} + \boldsymbol{B}$. Using simulation results of three operating conditions **A, B, C** in Table 5.1 (T_{eai}=26.7℃, T_{cai}=27.8 ℃, 35℃ and 39 ℃) and three condenser sizes (1, 2 and 4 times of original area A), a quantified relationship was proposed by linear curve fitting: $\Delta \boldsymbol{T_{sub}} = \boldsymbol{0.739^*} \Delta \boldsymbol{T_{in}} + \boldsymbol{0.227}$ (shown in Figure 5.1). With this relationship, COP maximizing subcooling temperature of the system studied in numerical analysis can be obtained for the specified conditions.

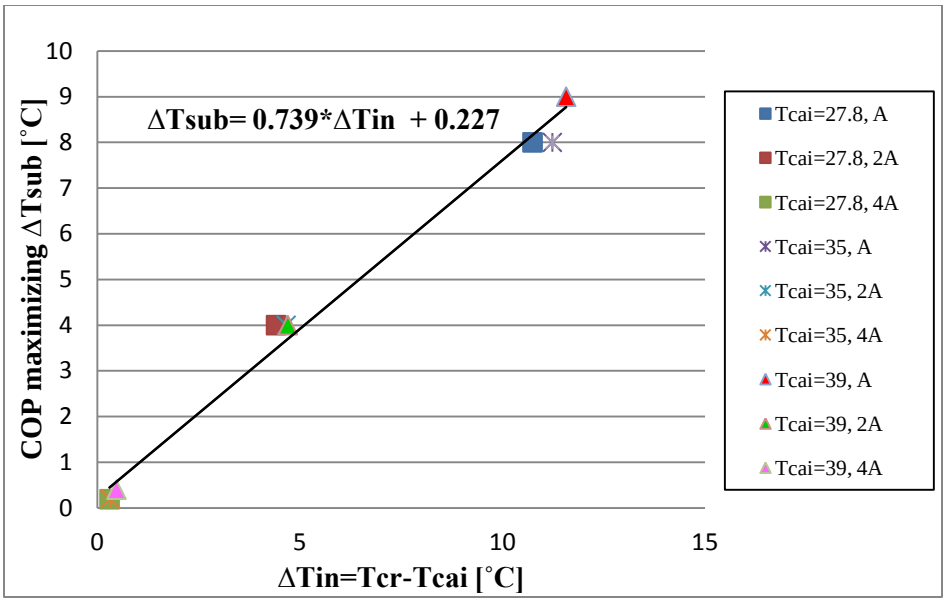

Figure 5.1: COP maximizing ΔT_{sub} as a linear function of condenser air refrigerant temperature difference ΔT_{in} for RAC system studied in numerical analysis

5.2 Maximization of cooling capacity Q

Same logic could be applied on capacity Q maximizing subcooling. Using the simulation results of three operating conditions **A, B, C** and three condenser sizes, a quantified relationship between Q maximizing subcooling temperature ΔT_{sub} and condenser air refrigerant temperature difference ΔT_{in} was obtained by linear curve fitting: $\Delta \boldsymbol{T_{sub}} = \boldsymbol{1.024}*\Delta \boldsymbol{T_{in}} + \boldsymbol{0.037}$ (shown in Figure 5.2). With this relationship, cooling capacity maximizing subcooling can be obtained for varying conditions.

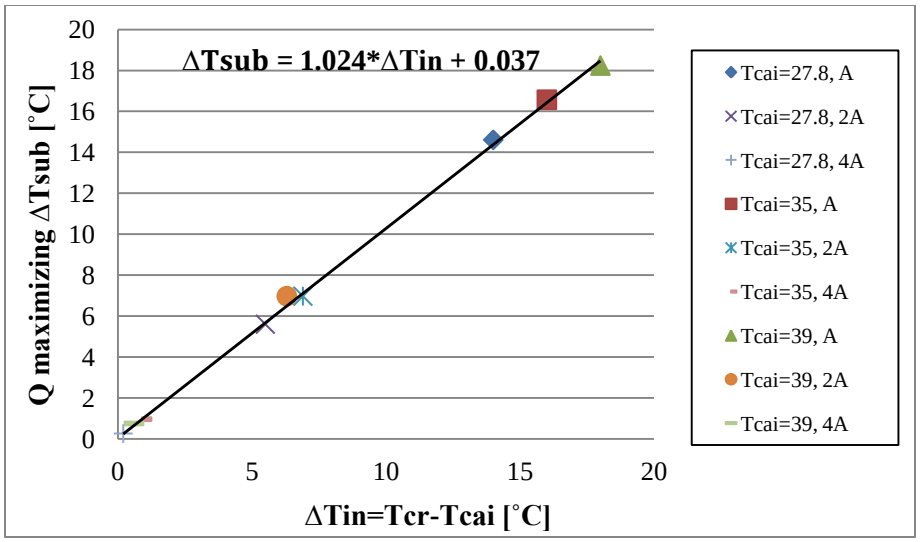

Figure 5.2: Q maximizing ΔT_{sub} as a linear function of condenser air refrigerant temperature difference ΔT_{in} for RAC system studied in numerical analysis

5.3 Generalization of COP maximizing subcooling control equation

Relationship developed in the previous section can be applied to a range of operating conditions and various condenser sizes for the refrigeration system studied in the simulation analysis. Experimental data in chapter 3 was added and combined with simulation results to see how well the quantified COP maximizing subcooling equation works for different refrigeration systems. As shown in Figure 5.3 (a), blue diamond symbol represents the behavior of RAC system using R410A from simulation results in chapter 4, red rectangle symbol represents the behavior of RAC system using R410A from experimental data in chapter 3. It seems that the control equation works pretty well for the RAC system in experimental study. The generalized control equation based on both simulation study and experimental data between COP maximizing subcooling temperature ΔT_{sub} and condenser air refrigerant temperature difference ΔT_{in} is obtained as: $\boldsymbol{\Delta T_{sub} = 0.727*\Delta T_{in} + 0.063}$ (Figure 5.3 (b)). This relationship is very similar to the correlation obtained based on simulation results alone.

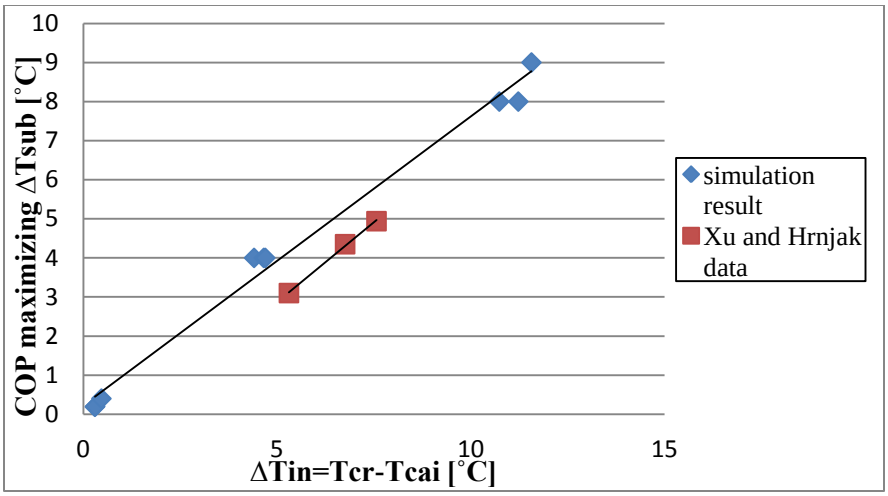

(a)

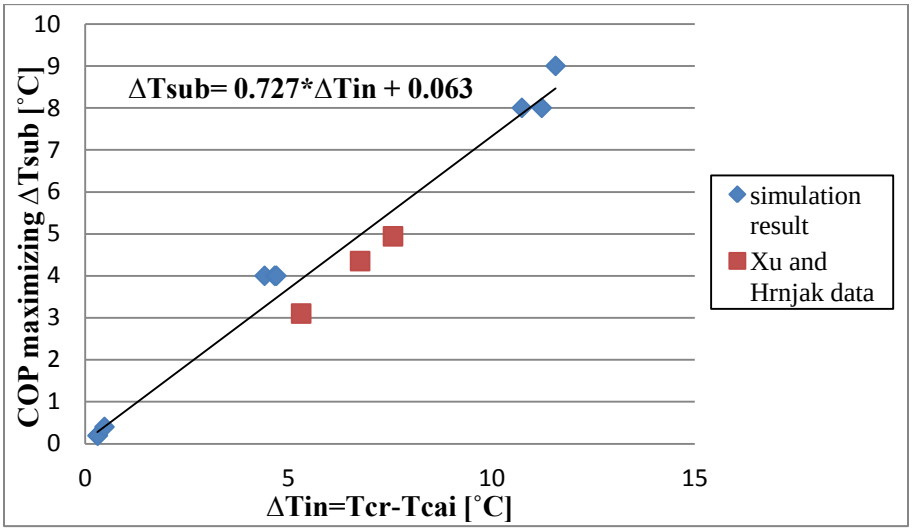

(b)

Figure 5.3: Generalized control equation between COP maximizing ΔT_{sub} and condenser air refrigerant temperature difference ΔT_{in} based on two refrigeration systems (a) three separate curve fit lines for each refrigeration system (b) one generalized curve fit line for three systems

The generalization of COP maximizing subcooling control equation was further tested with MAC system data from Pottker and Hrnjak (2012), represented by green triangle symbol in Figure 5.4 (a). It seems that the control equation follows the same trend for the MAC system but deviations are observed as a consequence of different component sizes (much smaller) and

refrigerants (R134a and R1234yf) in MAC system. The generalized control equation between COP maximizing subcooling temperature ΔT_{sub} and condenser air refrigerant temperature difference ΔT_{in} based on all three refrigeration systems was obtained: $\Delta T_{sub} = 0.502 * \Delta T_{in} + 0.932$ (Figure 5.4 (b)). This correlation is not perfect for general use in all the systems, indicating that each refrigeration system may require small tuning of the actual controller.

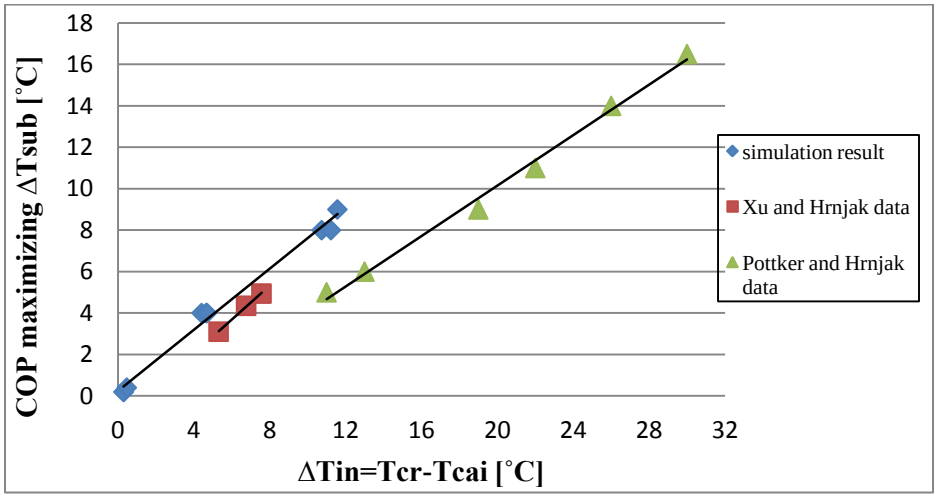

(a)

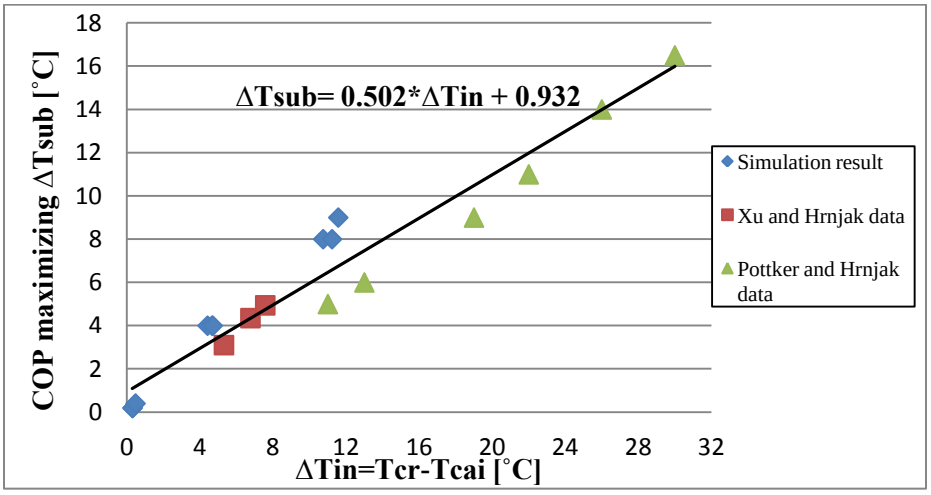

(b)

Figure 5.4: Generalized control equation between COP maximizing ΔT_{sub} and condenser air refrigerant temperature difference ΔT_{in} based on three refrigeration systems (a) three separate curve fit lines for each refrigeration system (b) one generalized curve fit line for three systems

5.4 Possible control algorithm

In principle there could be two objective functions for controlling subcooling: maximization of capacity Q and maximization of COP. In the previous section COP maximizing and Q maximizing values of subcooling have been presented. The correlation of COP or Q maximizing ΔT_{sub} as a function of condenser air refrigerant temperature difference ΔT_{in} is obtained for the RAC system studied in numerical analysis which hold for a range of component sizes (A, 2A, 4A as described in modeling section) and operating conditions (**A, B, C** in Table 4.3 and **D, E, F** in Table 3.3). A more generalized control equation is also obtained to extend the application of subcooling control strategy to different refrigeration systems while small tuning of real controller may needed.

If indicated values are attractive, a control can be obtained using an EXV (electronic expansion valve) after condenser to provide optimal subcooling for each condition. The strategy for controlling valve position can be based on maximization of capacity when needed (at the cool-downs or very high loads) followed by efficiency maximization once it is determined that capacity is sufficient.

The efficiency optimization procedure is presented in the flow chart in Figure 5.5. Based on measurements of condenser air inlet temperature T_{cai}, condensing temperature T_{cr}, and condenser refrigerant outlet temperatureT_{cro}, condenser air refrigerant temperature difference ΔT_{in} will be calculated. The COP maximizing subcooling value will be determined from the equation $\Delta \boldsymbol{T_{sub}} = 0.739 * \Delta \boldsymbol{T_{in}} + 0.227$ (Figure 5.1) and compared with the actual subcooling temperature. If the actual value is bigger than the curve-fitting value, subcooling needs to be decreased. EXV will be adjusted in the direction of opening it more so that condensing pressure will decrease. The lowering of condensing pressure will enlarge the two-phase region of

condenser during heat transfer and thus reduce subcooling. Vice versa for the case that actual subcooling is smaller than the ideal value. EXV needs to be adjusted in the direction of closing it. If capacity is not sufficient, maximization of capacity will be applied. The capacity optimization procedure is the same as efficiency optimization except that the Q maximization subcooling value is calculated using equation $\Delta T_{sub} = 1.024*\Delta T_{in} + 0.037$ (Figure 5.2). If automatic adjusting of EXV can be achieved, the residential a/c system will be able to maintain COP or Q maximizing subcooling when conditions change.

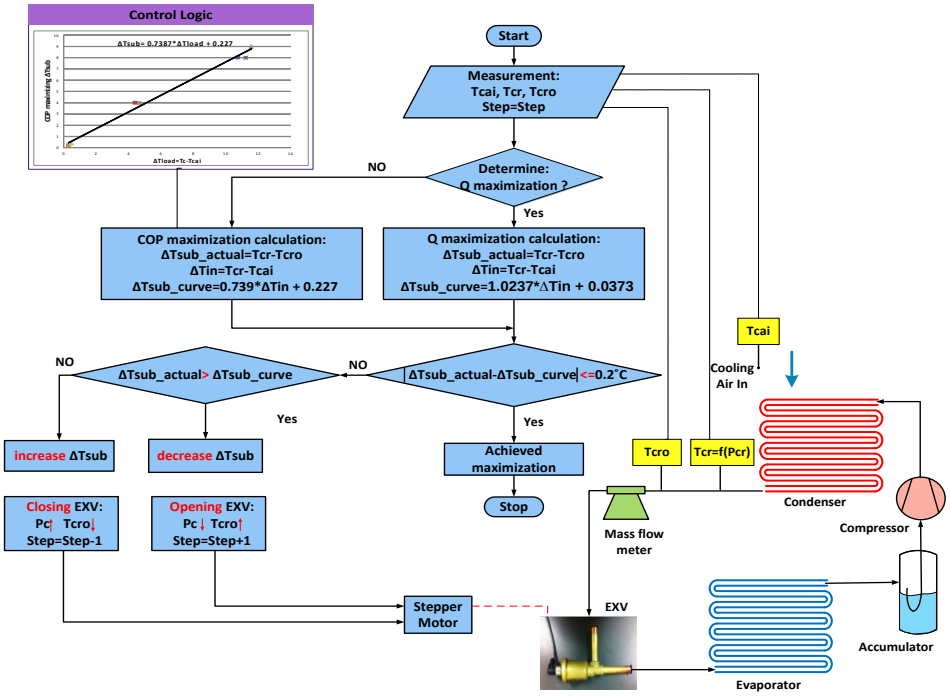

Figure 5.5: Control strategy

CHAPTER 6- SUMMARY AND CONCLUSIONS

In conclusion, numerical study and experimental study have both confirmed that system performance (COP and cooling capacity Q) can be improved by controlling subcooling using EXV for RAC system compared to conventional superheat controlled TXV system. The maximum COP improvement achieved is 33.0% and maximum Q gain is 14.7% from experiments at the same optimum subcooling, benefited from both subcooling control and improved evaporator effectiveness. The efficiency improvement in experiments is much higher than the 8% improvement from simulation model mainly because the improving of evaporator effectiveness due to reduced superheat/dry-out was disregarded in the simulation model.

Both simulation and experimental results indicated that COP maximizing subcooling temperature increases with increasing ambient temperature T_{cai}. In addition, the simulation evaluation in chapter 4 showed that subcooling effect is also affected by condenser sizes: smaller size of condenser is more sensitive to subcooling effect and COP maximzing subcooling deceases with increasing condenser sizes. The subcooling effect and condenser size effect were both interpreted as effect of condenser air refrigerant temperature difference ΔT_{in} on subcooling improved system performance. Higher ambient temperature and smaller condenser size both results in higher ΔT_{in} and thus greater room for condenser subcooling and consequently greater potential for COP or Q improvements. In fact, COP or Q maximizing subcooling temperature can be represented as a linear function of ΔT_{in} and subcooling can be controlled to achieve the optimal value.

In reality, the charge of the system is usually set; the condition changes, subcooling may not be at the COP or Q maximizing value. If automatic control of subcooling can be achieved, COP or Q maximization will be ensured. This study proposed one way of controlling subcooling using

an EXV with ΔT_{in} (temperature difference between inlet air and condensing refrigerant) as input signal for controlling subcooling (adjusting the EXV opening). The identified parameter ΔT_{in} also indicates the type of sensor that should be used in the implementation of the concept. This study also presented correlations to maximize efficiency (Figure 5.1) or cooling capacity (Figure 5.2) for the RAC system explored in simulation study from chapter 4 as well as a generalized correlation to maximize efficiency for three different refrigeration systems by combining the simulation results with experimental data from chapter 3 and with experimental data in Pottker and Hrnjak (2012). The generalized equation obtained is not perfect for all refrigeration systems due to different component sizes and refrigerants used, but the small deviations could be either neglected or fine-tuned in real applications.

APPENDIX

1. Results for other two conditions of condenser size effect in chapter 4 (keeping air face velocity constant by multiplying volumetric flow rate same factor as condenser size):

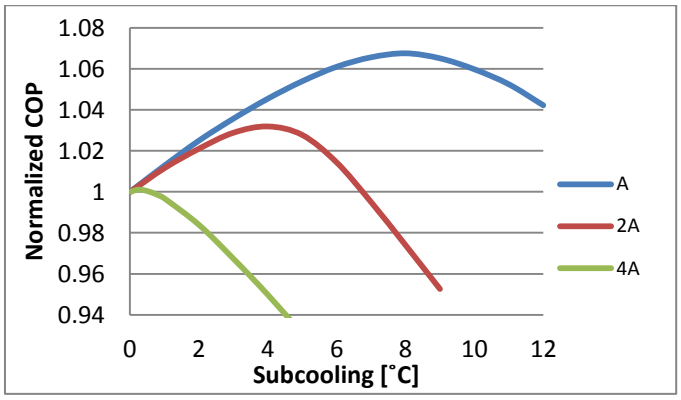

Figure A.1: Condenser size effect on COP (condition **A** in Table 4.3)

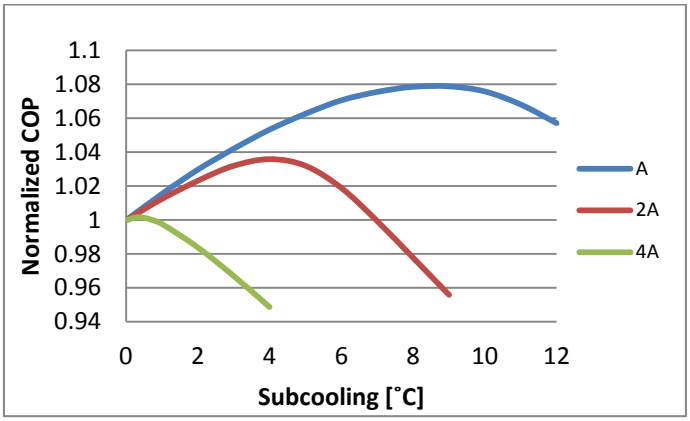

Figure A.2: Condenser size effect on COP (condition **C** in Table 4.3)

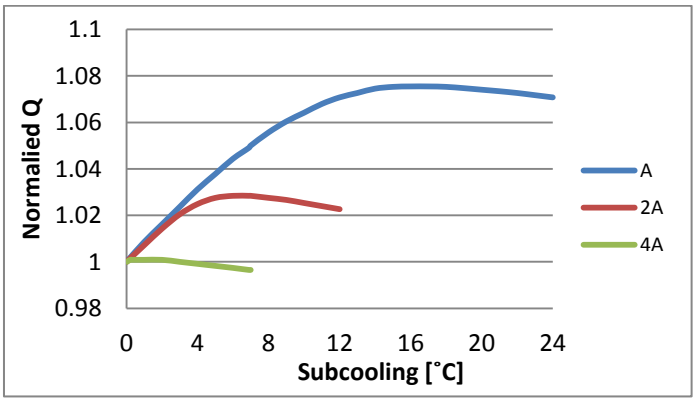

Figure A.3: Condenser size effect on Q (condition **A** in Table 4.3)

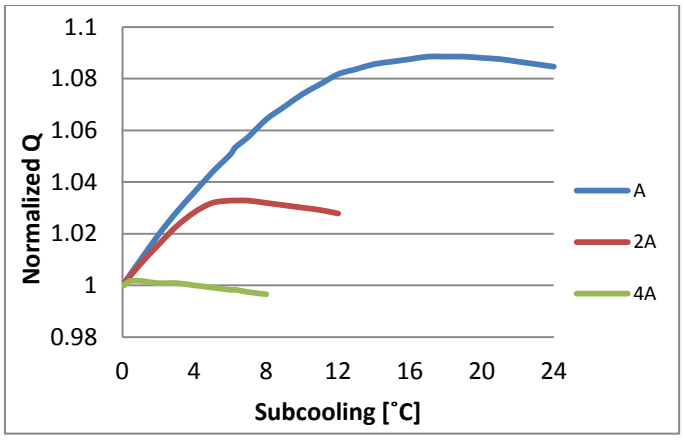

Figure A.4: Condenser size effect on Q (condition **C** in Table 4.3)

2. Results for three conditions of condenser size effect in chapter 4 (keeping air volumetric flow rate constant):

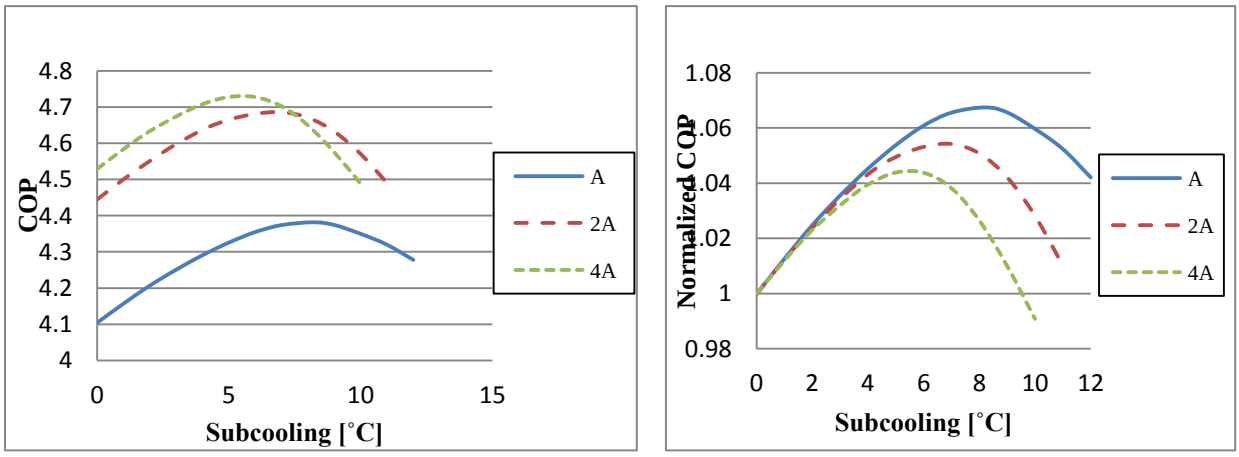

(a) (b)

Figure A.5: Effect of condenser size on subcooling improved COP presented in (a) actual and (b) normalized terms (condition **A** in Table 4.3)

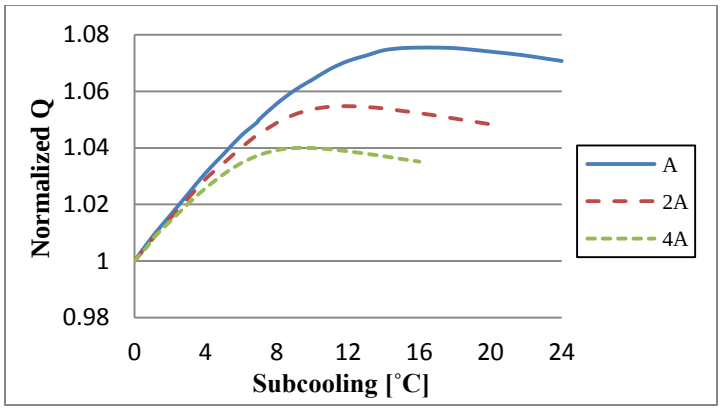

Figure A.6: Effect of condenser size on subcooling improved cooling capacity Q presented in normalized way (condition **A** in Table 4.3)

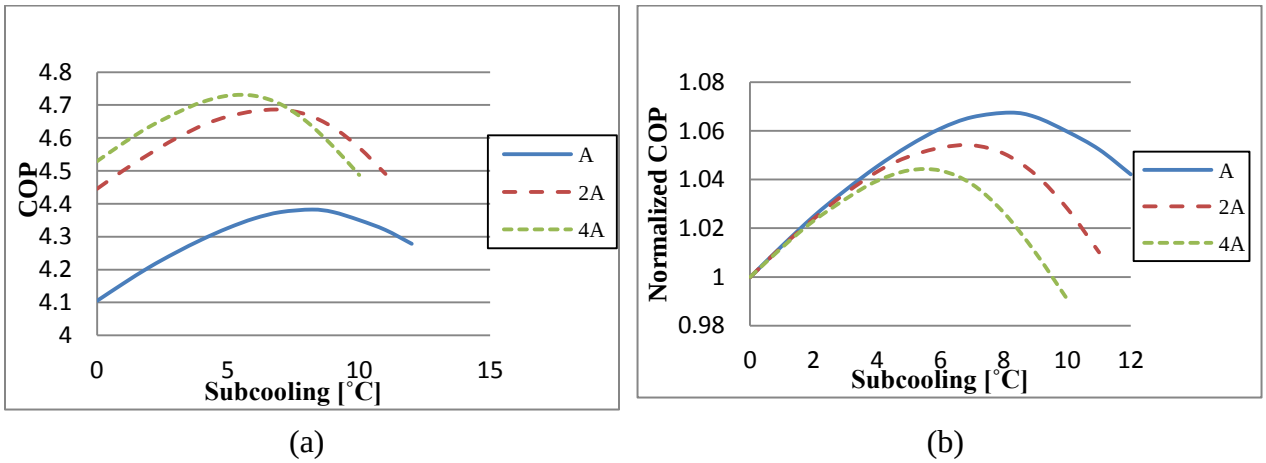

(a) (b)

Figure A.7: Effect of condenser size on subcooling improved COP presented in (a) actual and (b) normalized terms (condition **B** in Table 4.3)

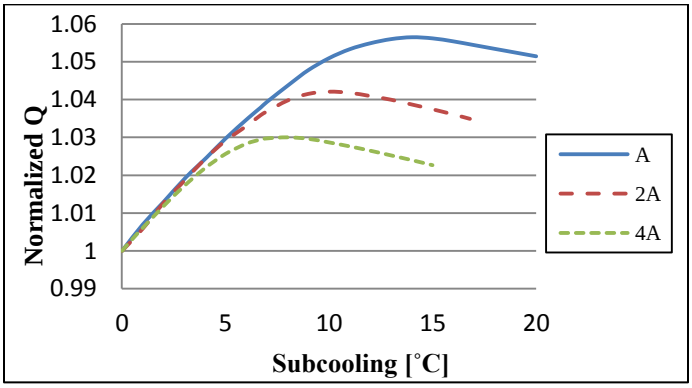

Figure A.8: Effect of condenser size on subcooling improved cooling capacity Q presented in normalized way (condition **B** in Table 4.3)

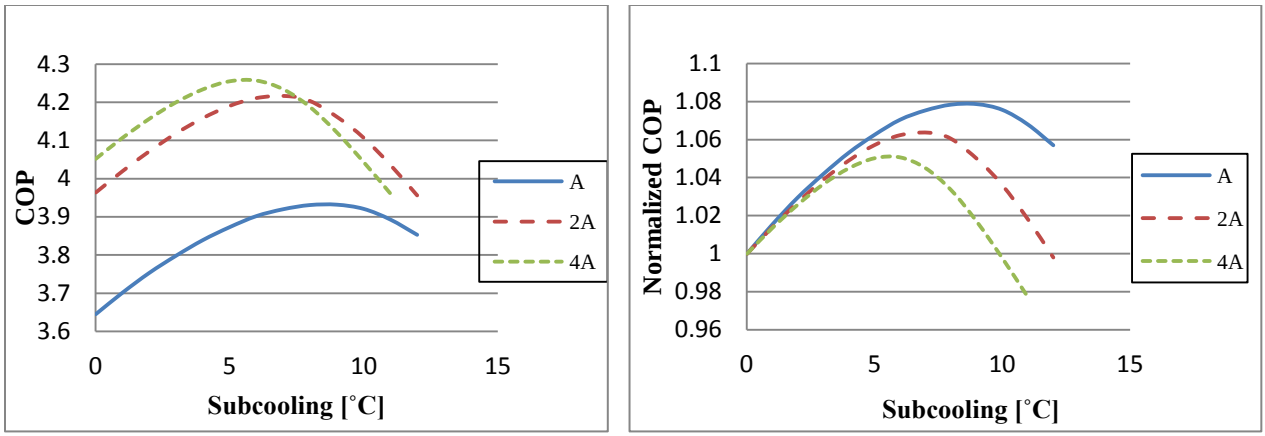

(a) (b)

Figure A.9: Effect of condenser size on subcooling improved COP presented in (a) actual and (b) normalized terms (condition **C** in Table 4.3)

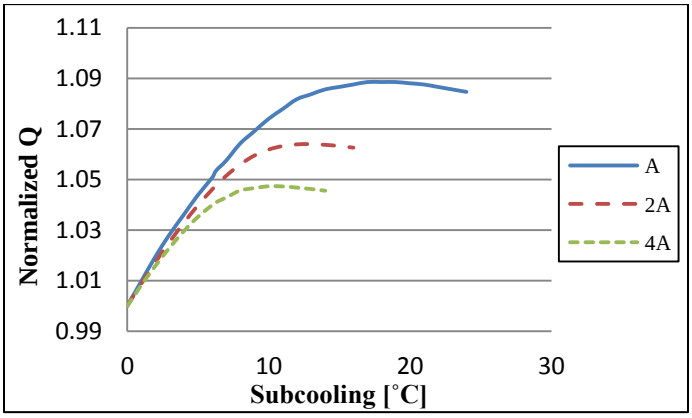

Figure A.10: Effect of condenser size on subcooling improved cooling capacity Q presented in normalized way (condition **C** in Table 4.3)

REFERENCES

ANSI/ASHRAE Standard 116, 1995. Method of testing for seasonal efficiency of unitary air-conditioners and heat pumps, Proceeding American Society of Heating, Refrigeration and Air-Conditioning Engineers.

Beaver, A.C., Yin, J.M., Bullard, C.W., Hrnjak, P.S., 1999. An experimental investigation of transcritical carbon dioxide systems for residential air conditioning. *University of Illinois at Urbana-Champaign*, ACRC CR-18.

Cavallini, A., Del Col, D., Doretti, L., Matkovic, M., Rossetto, L., Zilio, C.,Censi, G., 2006. Condensation in horizontal smooth tubes: a new heat transfer model for heat exchanger design, *Heat Transfer Engineering* 27 (8), 31-38.

Churchill, S.W., 1977. Friction-factor equation spans all fluid-flow regimes, *Chemical Engineering* 84.

Friedel, L., 1979. Improved friction pressure drop correlations for horizontal and vertical two phase pipe flow. *In: European Two Phase Flow Group Meeting*, Italy, Paper E2.

Gnielinski, V., 1976. New equations for heat and mass transfer in turbulent pipe and channel flow, *International Chemical Engineering* 16, 359–368.

Li. H, Hrnjak, P.S., 2013, Effect of lubricant on two-phase refrigerant distribution in microchannel evaporator, *SAE International Journal of Materials and Manufacturing*, vol. 6.

Li, H., Hrnjak, P.S., 2014. An experimentally validated model for microchannel heat exchanger incorporating lubricant effect. *Int Refrig and Air Conditioning Conf at Purdue*, No. 2148.

Kim, N.H., Yun, J.H., Webb, R.L., 1997, "Heat transfer and friction correlations for wavy plate fin-and-tube heat exchangers, *Transactions of ASME*, vol. 119, 560-567.

Pottker, G, Hrnjak, P.S., 2012.Potential for COP Increase in Vapor Compression Systems. *University of Illinois at Urbana-Champaign*, ACRC TR-294.

Pottker, G, Hrnjak, P.S., 2014. Effect of the condenser subcooling on the performance of vapor compression systems, *International Journal of Refrigeration*, doi:10.1016/j.ijrefrig.2014.11.003.

Pottker, G, Hrnjak, P.S., 2014. Experimental investigation of the effect of condenser subcooling in R134a and R1234yf air-conditioning system with and without internal heat exchanger, *International Journal of Refrigeration*, doi:10.1016/j.ijrefrig.2014.10.023.

Wallelet, J.P. et al., 1994. Heat transfer flow regimes of refrigerants in a horizontal-tube evaporator, *University of Illinois at Urbana-Champaign*, ACRC TR-55.

Webb, R.L., 1990. Air-side heat transfer correlations for flat and wavy plate fin-and tube geometries, *ASHRAE Transactions*, Vol.96, 445-449.